Capture of gaseous iodine in isoreticular zirconium-based UiO-n Metal-Organic Frameworks: influence of amino functionalization, DFT calculations, Raman and EPR spectroscopic investigations

Maeva Leloire,[a] Catherine Walshe,[a] Philippe Devaux,[a] Raynald Giovine,[a] Sylvain Duval,[a] Till Bousquet,[a] Siwar Chibani,[a] Jean-Francois Paul,[a] Alain Moissette,[b] Hervé Vezin,[b] Philippe Nerisson,[c] Laurent Cantrel,[c] Christophe Volkringer,[a] Thierry Loiseau*[a]

[a] Université de Lille, Centrale Lille, ENSCL, Univ. Artois, UMR CNRS 8181-UCCS, Unité de Catalyse et Chimie du Solide, 59000 Lille, France.
[b] Université de Lille, UMR CNRS 8516-LASIRE, Laboratoire de Spectroscopie pour les Interactions, la Réactivité et l'Environnement, 59000 Lille, France.
[c] Institut de Radioprotection et de Sûreté Nucléaire (IRSN), PSN-RES, 13115 Saint Paul lez Durance, France.

Accepted in *Chem. Eur. J.* e202104437 28 (2022)
Version december 13, 2021
Revised version January 14, 2022

ABSTRACT: The series of Zr-based UiO-n MOF materials (n = 66, 67, 68) have been studied for the iodine capture. The gaseous iodine adsorption has been collected kinetically from an home-made set-up allowing the continuous measurement of iodine content trapped within UiO-n compounds, with organic functionalities (-H, -CH_3, -Cl, -Br, -$(OH)_2$, -NO_2, -NH_2, -$(NH_2)_2$, -CH_2NH_2) by in-situ UV-Vis spectroscopy. This study emphasizes the role of the amino groups attached to the aromatic rings of the ligands connecting the $\{Zr_6O_4(OH)_4\}$ brick. In particular, the preferential interaction of iodine with lone electron pair groups, such as amino functions have been experimentally observed, and is also based on the DFT calculations. Indeed, higher iodine contents were systematically measured for the amino-functionalized UiO-66 or UiO-67, compared to the pristine ones (up to 1211 $mg.g^{-1}$ for UiO-67_$(NH_2)_2$). However, DFT calculations have revealed the highest computed interaction energies for the alkylamine groups (-CH_2NH_2) in the UiO-67 (-128.5 $kJ.mol^{-1}$ for octahedral cavity), and pointed out the influence of this specific functionality versus aromatic amine. The encapsulation of iodine within the pore system of UiO-n and their amino-derivatives has been analyzed by UV-Vis and Raman spectroscopy. We showed that a systematic conversion of molecular iodine (I_2) species into anionic I^- one, (stabilized as $I^- \cdots I_2$ or I_3^- complex within the MOF cavities), occurs when I_2@UiO-n samples are left in ambient daylight.

KEYWORDS. *UiO-n MOF materials; gaseous iodine adsorption; kinetics; Raman spectroscopy; EPR spectroscopy; DFT calculations*

1. INTRODUCTION

The recent Fukushima-Daiichi severe accident reminds us that the nuclear industry is still requiring developments in order to limit the risk and the environmental impact of an accident in the field of energy production.[1,2] Radioiodine (mainly ^{129}I and ^{131}I) is identified as one of the most toxic volatile species generated by a fission reaction. Its dangerousness is mainly associated to the volatility of iodine derivatives, as well as the biological affinity towards human body. So far, specific installations were already developed in nuclear plants for the capture and the immobilization of radioactive iodine. They involve scrubbing methods as well as porous solid materials like silver-doped zeolites of activated charcoals.[3]

Based on their large porosity and chemical versatility, Metal-Organic Frameworks (MOFs) materials appear well adapted to be used in such accidental conditions and can represent a suitable alternative to zeolites, charcoal having a too low auto-ignition point.[4–6] Furthermore, MOFs can show a great chemical resistance, since they can be stable in liquid water, at high temperature under steam or under irradiation. Previous studies have thus shown a significant stability of MOF materials networks when irradiated under large gamma ray doses.[7–10] Therefore, right after the events of Fukushima, the first studies about the capture of radionuclides in MOFs emerged in the literature. These species can be solubilized in water like actinides, technetium and cesium,[4,11] or gaseous like noble gas (Xe, Kr)[12] iodine derivatives.[13]

In the case of molecular iodine, the first studies were performed with ZIF-8(Zn).[14] This particular MOF compound was mainly selected for its pore aperture that fits very well with the size of I_2, allowing the good immobilization of this molecule within the framework. This confinement is permanent when the iodine loaded MOF is pressed until amorphization[15] or mixed with a low-temperature sintering material to form a stable glass composite.[16]

In parallel to the control of the pore size, the functionalization is found to be an alternative method to favor the confinement of iodine molecules within the pores. In 2013, our group demonstrated that electron donor groups attached to the frameworks induce the formation of a charge transfer complex between the MOF and molecular iodine.[17] Such functions can be connected to the organic ligand or related to hydroxyl bridges linking metallic cations. This affinity for iodine is easily explained by the electron donor character of the chemical function (especially $-NH_2$ and -OH), leading to the polarization of the electron cloud of iodine molecule. Other works take advantage of this strategy and allow records for iodine uptake within MOFs, up to 1.54 $g.g^{-1}$.[5,18] Higher iodine loading of 1.75 $g.g^{-1}$ was reported in the classic HKUST-1[19] and a maximal uptake of 2.79 $g.g^{-1}$ has been observed in the UiO-n analog of interpenetrated isoreticular networks based on the 4,4'-[1,4-phenylenebis(ethylene-2,1-diyl)]-dibenzoate linker.[20] In our recent contribution, we also described the good stability of the UiO-66_NH_2 compound trapping radioactive ^{131}I isotope exposed to severe conditions (120°C, humid gas flux, gamma irradiation).[21]

Despite these stimulating results, highlighted either the importance of functionalization and/or the pore aperture,[13] we may point out that there are few works reporting the adsorption of iodine under its gaseous form within MOF materials. Indeed, in the present study, we focused our efforts on the systematic investigations of gaseous iodine adsorption in the zirconium-based UiO-n archetype. These compounds constructed from the hexanuclear $\{Zr_6O_4(OH)_4\}$ poly-

oxo/hydroxo cluster, offer a great opportunity to study the combined effect of porosity and functionalization for the molecules capture. This well-known MOF family has been previously studied for its iodine sorption kinetic properties by analyzing the influence of different parameters, such as the impact of structure defects in UiO-66,[22] the addition of alkyne group on the ditopic carboxylate linker in UiO-n derivatives,[20] the functionalization of the amino group by barbituric or thiobarbituric acid group in UiO-66_NH_2,[23] or the effect of the structural types related to the occurrence of hexanuclear $\{Zr_6O_4(OH)_4\}$ bricks (UiO-66, UiO-67, MOF-808, NU-1000).[24] These reports dealt with the use of iodine vapor generated in a closed cell, in contact with the considered powdered UiO-n compounds, which are then weighted for the estimation of iodine uptake. For this UiO-n series, other works also described the influence of defects in the Hf-UiO-66 solids[25] or the effects of the nature of a wide variety of functional organic groups decorating the ditopic ligands in UiO-66,[26] by analyzing the iodine sorption from liquid phase using cyclohexane as solvent.

The aim of the present contribution is the investigation of the kinetics of gaseous iodine adsorption of the series of Zr-UiO-n. Indeed, the porosity of these solids can be tailored by varying the size of the ligand as well as by the chemical groups attached to them. We have paid a special attention to the study of the influence of the nature of decorating organic groups (-CH_3, -Cl, -Br, -$(OH)_2$, -NO_2, -NH_2) on the terephthalate ligands for UiO-66, and the effect of amino groups addition for the isoreticular UiO-67 or UiO-68 compounds. In particular, we have considered the configurations with the amino (-NH_2 or (-NH_2)$_2$) groups or alkylamino (-CH_2NH_2) groups attached to the benzene ring of the ditopic carboxylate ligand in the UiO-67 type. In these structures, the hexanuclear $\{Zr_6O_4(OH)_4\}$ units are connected to each other via a dicarboxylate ligand separated by one (UiO-66), two (UiO-67) or three benzene rings (UiO-68) (Figure 1). Their crystal structures give an estimated range of pore diameter (triangular window) from 6 up to 10 Å[27] and large cages (octahedral cavity) ranging from 11 Å (UiO-66),[28] 17 Å (UiO-67)[29] to 23 Å (UiO-68).[30]

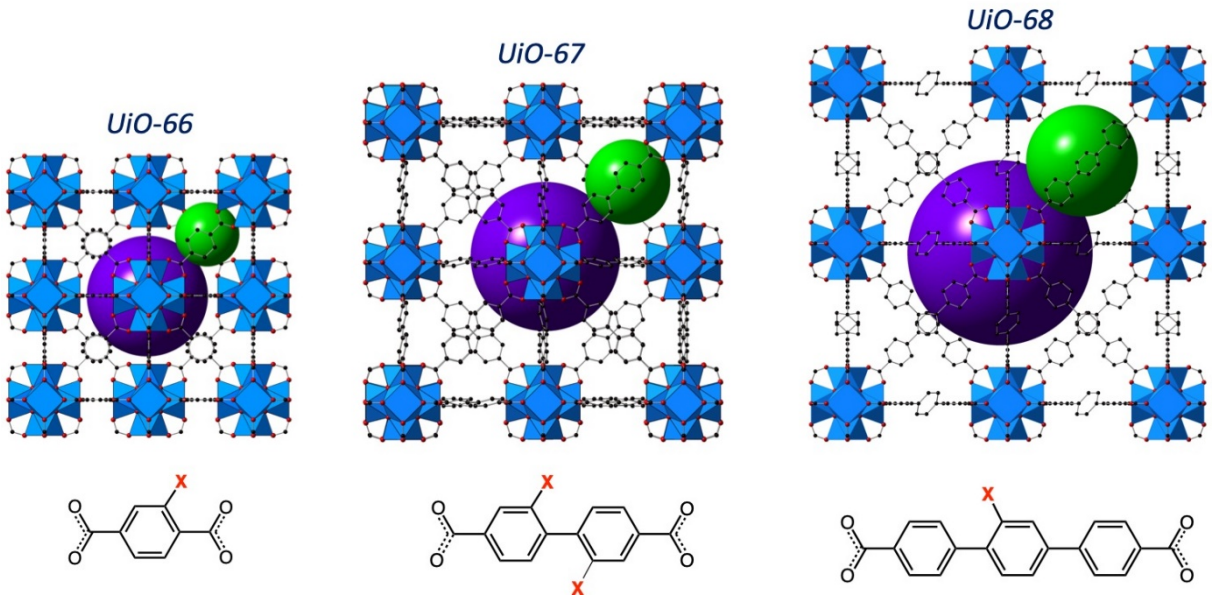

Figure 1. Illustrations of the UiO-66, UiO-67 and UiO-68 structures and the ligands derived from BDC (1,4-benzene-dicarboxylate), BPDC (4,4'-biphenyldicarboxylate) and TPDC (para-terphenyl-4,4"-dicarboxylate), used for their syntheses. The site(s) of ligand functionalization is marked in red, and corresponds to R = -H, -CH_3, -Cl,

-Br, $-NH_2$, -OH, $(-NH_2)_2$, $-CH_2NH_2$, according to the selected ligand. The sites of octahedral (noted OCTA) and tetrahedral (TETRA) cavities found in UiO-n archetypes, are represented by violet and green spheres, respectively.

These solids and their functionalized versions were used as a filter in a home-made installation, for the capture of gaseous iodine at room temperature. For this purpose, we designed a specific set-up containing a production unit of iodine vapor, which is transferred into a cell containing a powdered MOF solid using an argon gas flow. The iodine/Ar flux is then measured continuously by UV-Vis spectroscopy, generating an iodine uptake curve as a function of exposure time.

The synthesis of the different versions of UiO-n compounds as well as the unconventional organic ligands are described. The UiO-n solids are then characterized by classical techniques such as powder X-ray diffraction and Brunauer-Emmett-Teller (BET) surface area analysis. The kinetic curves of gaseous iodine will be discussed in terms of the nature of functional groups or pore sizes. Thereafter, the iodine-loaded solids I_2@UiO-n, were characterized by a combination of spectroscopic techniques, including UV-Vis, Raman (including microscopic mapping) and Electron Paramagnetic Resonance (EPR), in order to understand the iodine capture process as well as its kinetic conversion into anionic I_3^- species. These results were confronted to Density Functional Theory (DFT) calculations, which model the interaction of the adsorption molecule and the UiO-n frameworks to estimate the interaction energies taking into account either electron transfers and van der Waals effects, and correlated to the trapped iodine release temperature (from thermogravimetric analysis).

2. EXPERIMENTALS METHODS

2.1. UiO-n synthesis.

The synthesis of the different Zirconium-based UiO-n compounds was inspired from the published procedures and reported in supplementary information.[27] Only one UiO-67 member containing the $-CH_2NH_2$ functionalization has been previously published in literature and its synthesis was described in details (Supporting Info S1-S3).

2.2. UiO-n characterization.

The series of UiO-n compounds have been characterized by powder X-ray diffraction and nitrogen adsorption at 77 K in order to estimate the specific surface area and porosity volume. The corresponding powder XRD patterns are compared to each non-functionalized UiO-n type (UiO-66, UiO-67 and UiO-68) and do not exhibit any Bragg peak assigned to crystallized ligands or other phases. They are gathered in supplementary information (Supporting Info S5). The specific surface area values of the whole series of UiO-n studied in the present work, have been obtained from the activated forms (Supporting Info S4), according to the BET (Brunauer-Emmett-Teller) model (S_{BET}) and listed in Tables 1 and 2. The parameters used for calculations are described in the supporting information (S6). The S_{BET} values of the UiO-66 (noted UiO-66_H) and derivatives samples correspond to synthesis batches using formic acid as modulators. The non-functionalized UiO-66_H exhibits a S_{BET} value of 1387 $m^2.g^{-1}$ with a pore volume of 0.56 $cm^3.g^{-1}$. The addition of diverse functionalities on the aromatic ring gives rise to the decrease from 1166 down to 610 $m^2.g^{-1}$, for UiO-66_CH_3 and UiO-66_$(OH)_2$,

respectively. These S_{BET} values are in the expected range for such solids as reported in literature.[31] The pore volume values follow the same trend. The UiO-67 solid (obtained with the HCl modulator) possesses a S_{BET} value of 1599 $m^2.g^{-1}$, which is lower than the optimal value announced at 2500 $m^2.g^{-1}$ in literature (using a similar synthetic procedure.[32] This difference might be due to the lower stability of the UiO-67 archetype together with the utilization of a mild activation process in order to avoid its framework collapse. The functionalized UiO-67 compounds have been prepared in the presence of benzoic acid as modulator. UiO-67_NH_2 has a S_{BET} value of 1565 $m^2.g^{-1}$, similar to that measured for the unfunctionalized UiO-67. The compounds UiO-67_$(NH_2)_2$ and UiO-67_CH_2NH_2 have lower S_{BET} values of 1109 and 1112 $m^2.g^{-1}$, respectively. As mentioned previously with UiO-67, the low stability of UiO-68_NH_2 (also synthesized with benzoic acid modulator) did not allow us to access maximal porosity, which is theoretically estimated at 4710 $m^2.g^{-1}$.[33] In addition, to our knowledge, no study reports an experimental value of the S_{BET} for the compound UiO-68_NH_2 (1054 $m^2.g^{-1}$ in our work).

2.3. I_2 gas-phase dynamic sorption.

The adsorption capacity of the selected UiO-n compounds towards I_2 was investigated using a dedicated experiment. The experimental setup devoted to I_2 sorption test can be divided in three main parts: the generation of the I_2 inlet flow, a fixed–bed glass reactor and the quantification system composed of bubblers containing potassium iodide solution (KI, 0.1 M) and an UV-Vis spectrometer for the continuous analysis of iodine uptake. Details of the setup are indicated in Supporting Info S7.

Prior to analysis, UiO-n solids were thermally treated in order to remove trapped species within the pores and immediately transferred into a glove box (under Ar) in order to avoid any contamination during the preparation of the sample (Supporting Info S4). Within the glove box, 30 mg of activated UiO-n is transferred within the glass sintered cell, leading to a 1 cm bed height. At the end of the experiment, the iodine-loaded UiO-n compound is transferred into a glass vial and kept at -20°C in order to avoid any desorption of iodine.

2.3 Thermogravimetric analysis.

Thermogravimetric curves have been collected on the thermo-analyzer 92 SETARAM TGA up to 800°C under air flow, with a heating rate of 5°C.min^{-1}.

2.4 UV-Vis spectroscopy.

The UV-Vis experiment has been performed on a Varian Cary 5000 spectrometer using Praying Mantis™ Diffuse Reflection Accessory adapted for the characterization of powder samples. The spectra have been recorded in the 200-800 nm spectral range with a resolution of 1 nm. The diffuse reflectance spectra were plotted using the Kubelka-Munk function.

2.5 Raman spectroscopy.

The Fourier transform Raman spectra have been collected on a Bruker RFS 100/S type spectrometer using a 1064 nm excitation radiation (Nd:YAG laser), with a power of 50 mW. The Raman spectra have been recorded in the spectral range 50-3500 cm^{-1}, with a resolution of 2 cm^{-1}. The signal to noise ratio is acceptable for an accumulation number of the order of 600

scans. The 1064 nm excitation radiation allows to overcome both the intrinsic parasitic luminescence (fluorescence) of UiO-n compounds decorated with the amino functional group and the possible induced photoreaction of iodine (conversion of I_2 into I^- or I_3^-).[34]
Iodine mapping has been recorded with the Raman LabRam HR-Evolution micro-spectrometer (Horiba Scientific) using an Olympus 100 x 0.9 NA objective, allowing access to a spatial resolution of 1 µm. This spectrometer equipped with a holographic grating of 600 lines per mm, is coupled with three laser sources of wavelengths 473 nm, 515 nm and 633 nm. Spectral data is processed with LabSpec6 software. In order to collect Raman spectra and maps representative of the progress state, we chose to use the 633 nm excitation wavelength. This choice was motivated by the fact that this wavelength is not related to any absorption band of iodine species. In addition, to avoid any degradation of the single-crystal sample and not to photo-induce undesirable reactions of adsorbed iodine species, the laser power was set to its nominal value at 10%.

2.6 EPR spectroscopy.
X-band Continuous-Waver Electron Paramagnetic Resonance (CW-EPR) experiments were carried out at room temperature using a Bruker ELEXSYS E500 spectrometer. Kinetic measurements under light irradiation were performed in situ using a Hamamatsu LC8 irradiation lamp. CW spectra were collected using 1 G amplitude modulation and 1 mW microwave power.

2.7. DFT Calculations.
The evaluation of interaction energies between I_2 and the UiO-n family has been performed at the Density Functional Theory (DFT) level, using the Vienna Ab-initio Simulation Package (VASP).[35,36] The electron-ion interactions are described using the Projector Augmented Wave (PAW) method of Blöchl[37] adapted by Kresse and Joubert.[38] The calculations were done at the Γ-point only due to the large size of the unit cells. The gradient corrected exchange correlation functional of Perdew, Burke and Ernzerhof (PBE) was employed.[39] The DFT-D3 correction method of Grimme and co-workers[40] was used in the present work, as implemented in VASP by Moellmann et Grimme,[40–42] to estimate efficiently the dispersion forces. The wavefunction has been expanded in a plane wave basis set using a cutoff energy of 550 eV. The convergence parameters were set to 10^{-6} eV for the total energy and to 0.02 eV/Å for the residual forces on atoms. To improve electronic convergence, a Gaussian smearing with σ = 0.2 eV has been used. The interaction energies of iodine with the UiO-n structures are computed according to the following equation (1), E_{UiO} being the total energies of the clean UiO-n, E_{I2} the energy of the isolated $I_{2(g)}$ compounds and $E_{UiO\text{-}I2}$ the energy of the UiO-n network with adsorbed I_2 molecule. For our calculations, only pristine zirconium-based UiO-66/67/68 and amino-functionalized networks have been considered.

$$\Delta E_{int} = E_{UiO-I2} - E_{UiO} - E_{I2} \quad (1)$$

Similarly, the contribution of dispersion energy ΔE_{disp} to the interaction energy was computed in an analogous way:

$$\Delta E_{disp} = E_{disp-UiO-I2} - E_{disp-UiO} - E_{disp-I2} \quad (2)$$

In particular, we have used our recently optimized cell,[43] with the following parameters: $\alpha = \beta = \gamma = 90°$ and $a = b = c$ = 20.9 Å, 27.1 Å and 33.3 Å for UiO-66, UiO-67 and UiO-68, respectively.

3.1. Kinetic study of gaseous iodine sorption in UiO-66 series: influence of functionalization.

The kinetics of gaseous iodine adsorption by the UiO-66 (denoted UiO-66_H) compound and its functionalized analogs have been collected up to 48 h. Seven derivatives with diverse X functionalities have thus been investigated regarding the iodine sorption, denoted as UiO_X, with X = H, Cl, Br, CH_3, NO_2, $(OH)_2$, NH_2 and naphthalene (noted Napht). The kinetic curves have been analyzed by utilizing a simple analytic equation derived from the Linear Driving Force (LDF) model.[44] It has been successfully applied to the study of adsorption kinetics of gaseous species in MOF materials.[45–47] The LDF equation is given by:

$F(t) = 1 - \exp[-k_{LDF}t]$,

where $F(t)$ is the fractional uptake, expressed by the ratio of the uptake m_t (at time t) to the uptake m_{48h}, at t = 48 h, and k_{LDF} is the effective mass transfer coefficient (h^{-1} unit) at given temperature and pressure (in our case, ambient temperature and pressure). This model allows us to give the kinetic rates of iodine adsorption, for practical comparisons between the different UiO-n samples (Figure S81). It is thus observed that the fitting kinetic curves agree quite well with the experimental one (correlation coefficient R^2 in the range 0.980-0.997), except, surprisingly, for the compound UiO-66_H, for which a slight shift is observed between fitted and experimental curves (R^2 = 0.913).

The UiO-66_H compound exhibits a kinetic curve with a rapid iodine uptake (Figure 2), with nearly 90% of the capacity at $t \approx 12$ h, followed by a slower continuous uptake increase up to t = 48 h, with a I_2 capacity value of 210 $mg.g^{-1}$, and k_{LDF} = 0.229(4) h^{-1} (Table 1). The same kinetics behavior is observed for the functionalized UiO-66_X compounds, for which the saturation is always visible before t = 48 h. In general, higher kinetics rates are reported for the members X = Cl, Br, CH_3, NO_2 and Napht, with k_{LDF} values ranging from 0.267(2) h^{-1} (for UiO-66_Napht) up to 0.416(2) h^{-1} for UiO66_CH_3, with nearly 90% of the I_2 capacity in the range 5h30-8h40.

The lowest I_2 uptake at equilibrium is shown for UiO-66_Cl (171 $mg.g^{-1}$) and the largest for UiO-66_Napht (323 $mg.g^{-1}$). However, much higher iodine uptakes are observed for the UiO-66 decorated with hydroxo (UiO-66_$(OH)_2$; 388 $mg.g^{-1}$) or amino (UiO-66_NH_2; 565 $mg.g^{-1}$) group. The corresponding kinetics rates are 0.214 h^{-1} (closely related to that of UiO-66_H) and 0.0909(3) h^{-1}, respectively. For the amino-containing UiO-66 sample, the kinetics rates are twice as slow as compared to that of the unfunctionalized one (90% of the I_2 capacity reached after $t \approx 25$ h).

For this UiO-66 series, we noticed that the iodine uptake capacity does not correlate with the value of the BET specific surface area S_{BET} (or microporous volume). The highest S_{BET} value is associated to the unfunctionalized UiO-66_H (1387 $m^2.g^{-1}$), but with a maximum I_2 uptake of 210 $mg.g^{-1}$, whereas the highest amount of trapped iodine is 565 $mg.g^{-1}$ for the amino-decorated UiO-66 compound, which exhibits a S_{BET} of 825 $m^2.g^{-1}$. This indicates the drastic role of the nature of the functionality decorating the aromatic ring of the ditopic linker in the UiO-66 series, since higher iodine uptake is observed when amino groups are present.

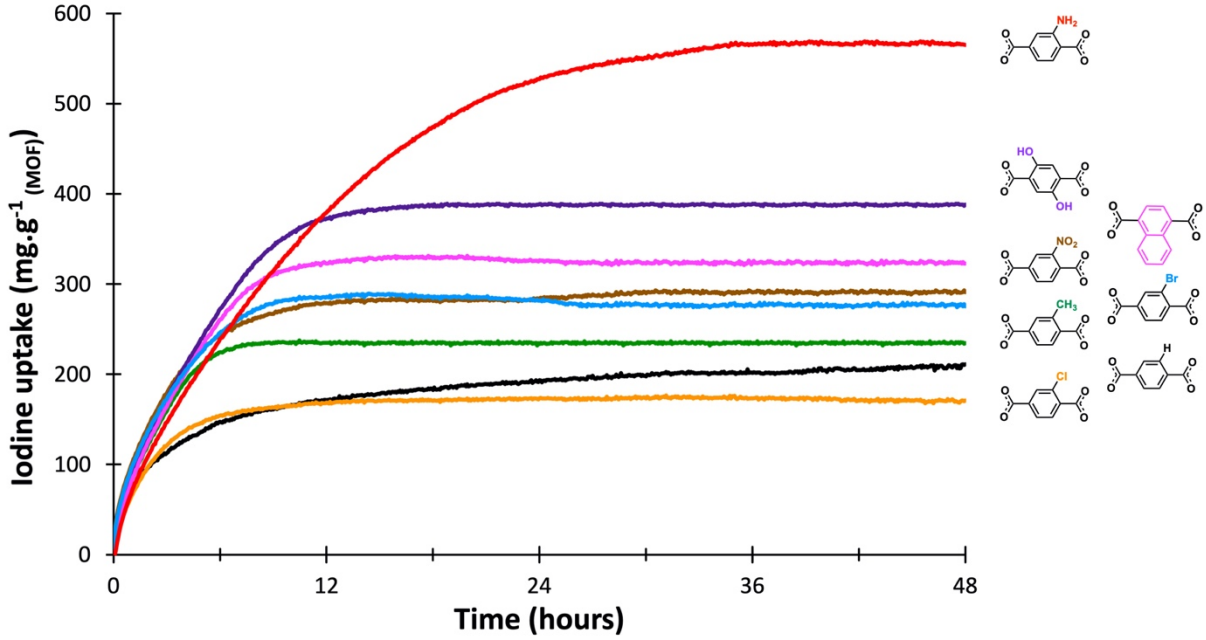

Figure 2. Experimental kinetic curve of gaseous iodine adsorption in UiO-66 derivative compounds, related to functionalized benzene groups belonging to the terephthalate linker. Adsorption have been carried out at room temperature and ambient pressure for an exposure time up to t = 48 h.

Table 1. BET specific surface area, microporous volume, iodine uptake capacities and fitted kinetic constants data for the UiO-66 series.

UiO-n	S_{BET} ($m^2.g^{-1}$)	Microporous volume ($cm^3.g^{-1}$)	Uptake capacity* ($mg_{I2}.g^{-1}$)	Uptake capacity* ($mol_{I2}.mol^{-1)}$)	k_{LDF} (h^{-1})	R^2	t (F = 0.90)*** (h)	t (F = 0.99)*** (h)
UiO-66_H	1387 ± 18	0,56	210	1.38**	0.229(3)	0.913	10h04	20h08
UiO-66_NH_2	825 ± 8	0,31	565	3.90	0.0909(3)	0.997	25h19	50h38
UiO-66_NO_2	741 ± 4	0,24	290	2.21	0.327(2)	0.987	7h02	14h04
UiO-66_Cl	843 ± 6	0,29	171	1.26	0.405(2)	0.991	5h40	11.36
UiO-66_$(OH)_2$	610 ± 3	0,18	388	2.83	0.214(1)	0.992	10h46	21h34
UiO-66_Napht	848 ± 5	0,26	323	2.50	0.267(2)	0.989	8h37	17h15
UiO-66_Br	739 ± 5	0,24	277	2.33	0.352(3)	0.980	6h32	13h05

UiO-66_CH_3	1166 ± 9	0,39	235	1.62	0.416(2)	0.993	5h31	11h03

*values obtained after 48 h I_2 loading; **not saturated kinetic curve at t = 48 h; k_{LDF}: mass transfer coefficient from the Linear Drive Force (LDF) model ($F(t) = 1 - \exp[-k_{LDF}t]$); R^2: correlation coefficient. ***Equilibration time t to reach F = 0.90 and 0.99 from LDF fit.

Previous experimental adsorption investigations[26] of molecular iodine in cyclohexane liquid phase, have shown similar results concerning the UiO-66_H, UiO-66_Br and UiO-66_NO_2 members. But they differed for the UiO-66_$(OH)_2$ and UiO-66_NH_2 compounds, for which identical higher iodine uptakes were reported. In our study, a significant difference iodine mass uptake of + 45% was observed for the UiO-66_NH_2 sample, despite of close S_{BET} values for both our solids. Moreover, other studies dealing with the gaseous iodine sorption in a close cell (static conditions with an iodine excess) for the pristine UiO-66 reported much higher capacities ranging from 660 $mg.g^{-1}$ [24] up to 1170 $mg.g^{-1}$ after 72 hours.[22] Such a disparity could be explained by the variable quantities of iodine used in the different studies. In fact, we worked with a total iodine amount of 38 mg (iodine rate of 0.8 $mg_{I2}.h^{-1}$) for about 30 mg of UiO-n sample (mass ratio close to 1), whereas the other authors reported larger iodine contents, with a mass ratio of 10 for I_2 related to UiO-n sample.[24]

In order to tentatively elucidate the different iodine uptakes within the UiO-66 framework and its functionalized derivatives, we assume that molecular iodine does weakly interact with the zirconium-centered polyoxo/hydroxo cluster, which constitutes an invariant parameter in our system. The latter being surrounded by organic ligands, is supposed to be less accessible due to their steric hindrance. Therefore, we started from the hypothesis (confirmed by the DFT calculations) that the iodine preferentially interacts with the organic linker, and particularly with the benzene ring, which offers a stronger affinity. The first interaction between an I_2 molecule and organic compound is of Van der Waals interaction type, but this interaction can be enhanced through the formation of charge transfer complex in the presence of benzene ring,[48–52] in particular when this latter is substituted with a -Br, -NO_2, -$(OH)_2$ or -NH_2 group.

The lower adsorption capacity of 171 $mg.g^{-1}$ for UiO-66_Cl, instead of 210 $mg.g^{-1}$ for UiO-66_H, can result from a lower electron density of the chloride-substituted aromatic.

However, the bromine function (UiO-66_Br sample) would probably favor the Br···I_2 through EDA-complexes formation. Experimental iodine adsorption shows that the UiO-66_Br compound is able to capture higher content with the value of 277 $mg.g^{-1}$, instead of 210 $mg.g^{-1}$ for UiO-66_H. The addition of a methyl group (UiO-66_CH_3) will slightly increase the van der Waals interactions and thus induced a little increase in iodine uptake (235 $mg.g^{-1}$) compared to UiO-66_H.

On the other hand, the UiO-66 compounds with the groups -NO_2, -OH, -NH_2 show higher iodine uptakes, with values of 290, 388 and 565 $mg.g^{-1}$ respectively. These high values reflect the charge transfer interaction between the lone electron pair on the functional groups and the I_2 molecule.

Finally, the rather acceptable iodine uptake with UiO-66_Napht sample (323 $mg.g^{-1}$) can be attributed to an increase in Van der Waals interaction compare to UiO-66_H.

3.2. Kinetic study of gaseous iodine adsorption in UiO-66 vs UiO-67 and UiO-68 series : influence of pore size and amino functionalization.

From the experience acquired on the UiO-66 type series, we extended our study to UiO-67 and UiO-68 solids, having larger pore size, and functionalizable by amino groups, which showed the best iodine uptakes in the previous UiO-66 series. We therefore focused our effort on the samples of UiO-67 framework and derivatives with different amino functionalizations: one -NH_2 function attached on the biphenyldicarboxylate linker (UiO-67_NH_2); two-NH_2 functions (UiO-67_$(NH_2)_2$; one methylamino group (UiO-67_CH_2NH_2). The UiO-68 solid has been considered for only the terphenyldicarboxylate linker bearing one amino group (-NH_2) in 2' position. The kinetic curves have been fitted by using the LDF model (Figures S82 & S83).[44] It is observed that the fitting kinetic curves agree quite well with the experimental one (correlation coefficient R^2 in the range 0.978-0.997), except, for the compounds UiO-67 and UiO-68_NH_2, for which the shifts are observed between fitted and experimental curves (R^2 = 0.924 and 0.951, respectively).

As expected, the unfunctionalized solid UiO-67 exhibits a low iodine adsorption capacity with a maximum value of 222 $mg.g^{-1}$ after t = 48 h, with a kinetic evolution (Figure 3) closely related to that of UiO-66_H (210 $mg.g^{-1}$), as well as with similar kinetic rate (k_{LDF} = 0.228(4) h^{-1}; Table 2). The insertion of an aminomethyl group (-CH_2NH_2) in UiO-67 framework induces the significant increase of iodine uptake with a value of 660 $mg.g^{-1}$ (after t = 48h). This gain is drastically further enhanced when the biphenyl-dicarboxylate linkers are decorated by a simple amino group (-NH_2), with a value of 1071 $mg.g^{-1}$ without reaching saturation at t = 48 h, and a k_{LDF} value of 0.0920(8) h^{-1} (twice smaller that than of UiO-67). The addition of a second amino group holds that highest iodine content within the pores of UiO-67_$(NH_2)_2$ for the present series, with the value of 1211 $mg.g^{-1}$, still without reaching the saturation after t = 48 h. These uptake values are comparable to that measured under static conditions, of ZIF-8 (1250 $mg.g^{-1}$),[14] or that reported by Maddock *et al.* in the pristine UiO-66 (1170 $mg.g^{-1}$),[22] but lower to that of HKUST-1 (1750 $mg.g^{-1}$).[19] The kinetic rates are identical for these two amino-decorated UiO-67 compounds, with k_{LDF} values of ≈ 0.0320(2) h^{-1}. Indeed, the presence of amino functions increases drastically the iodine uptake (up to 5-6 times factor), but is correlated by a much slower adsorption kinetics, with a rate divided by factor of ≈ 6. This correlation of the uptake versus kinetic rate is presumably controlled by the relatively low iodine flow of 0.2 $mg.h^{-1}$, used in our experimental set up. Finally, the compound UiO-68_NH_2 is able to adsorb a slightly higher amount of iodine (300 $mg.g^{-1}$) than UiO-67 (243 $mg.g^{-1}$), but much lower than UiO-67_NH_2 (1071 $mg.g^{-1}$), and is in the uptake range of UiO-n series, free of amino groups, but with slightly lower k_{LDF} value of 0.148(2) h^{-1}.

Once again, these kinetic evolutions point out the influence of the amino functionality, which promotes the iodine uptake capacities, although the pore cavity volume (from cage diameter of 17 Å for UiO-67 up to 23 Å for UiO-68) appears as an irrelevant parameter. Through these experiments the frameworks of UiO-67_NH_2 and UiO-67_$(NH_2)_2$ offer the best amino functionalization/porosity combinations for trapping iodine. The compound UiO-66_NH_2 also shows very good results, but its more limited cage volume (cage diameter of 11 Å) does not allow the same amount of guest iodine to be trapped. Conversely, the porous opening of UiO-68_NH_2 (cage diameter of 23 Å) seems too large and the concentration of amino functional groups too low, to retain a big amount of iodine.

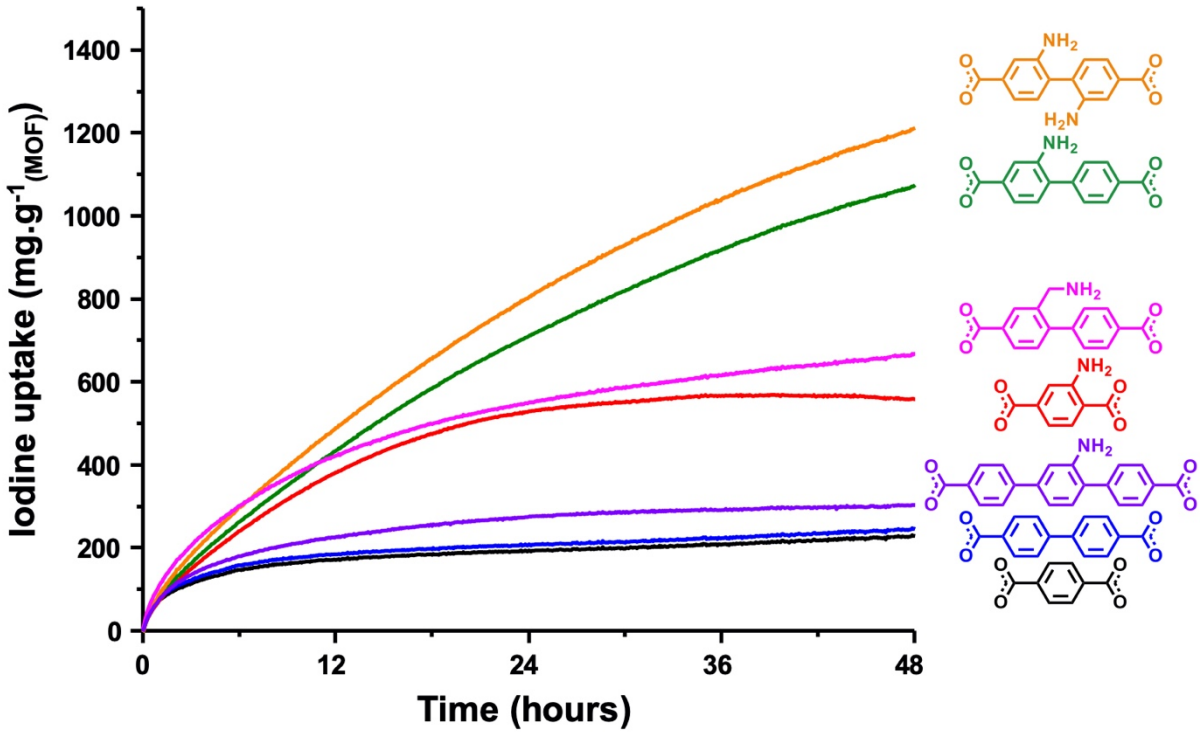

Figure 3. Kinetic curve of gaseous iodine adsorption in UiO-67 and UiO-68 derivative compounds, at room temperature, compared to that of UiO-66_H. Adsorption have been carried out at room temperature and ambient pressure for an exposure time up to t = 48 h.

Table 2. BET specific surface area, microporous volume, iodine uptake capacities and kinetic constants data for the UiO-n series.

UiO-n	S_{BET} ($m^2.g^{-1}$)	Microporous volume ($cm^3.g^{-1}$)	Uptake capacity* ($mg_{I2}.g^{-1}$)	Uptake capacity* ($mol_{I2}.mol^{-1}$)	k_{LDF} (h^{-1})	R^2	t (F = 0.90)*** (h)	t (F = 0.99)*** (h)
UiO-67	1599 ± 8	0,41	222	1.86**	0.228(3)	0.924	10h05	20h11
UiO-67_NH_2	1565 ± 3	0,83	1,071**	9.32**	0.0320(2)	0.997	72h02	144h06
UiO-67_$(NH_2)_2$	1109 ± 26	0,48	1,211**	10.97**	0.0319(2)	0.997	72h16	144h33
UiO-67 _CH_2NH_2	1112 ± 28	0,51	660**	5.96**	0.0920(8)	0.978	25h01	50h03
UiO-68_NH_2	1054 ± 12	0,38	300**	3.15**	0.148(2)	0.951	15h34	31h07

*values obtained after 48 h I_2 loading; **not saturated kinetic curve at t = 48 h; k_{LDF}: mass transfer coefficient from the Linear Drive Force (LDF) model ($F(t) = 1 - \exp[-k_{LDF}t]$); R^2: correlation coefficient. ***Equilibration time t to reach F = 0.90 and 0.99 from LDF fit.

3.3. Study of the thermal desorption of trapped iodine in UiO-n compounds and DFT calculations.

In order to investigate the retention of iodine trapped within the cavities of UiO-n compounds, we measured its temperature of release by thermogravimetric analysis. Only a selection of

iodine-loaded UiO-n samples have been studied, and is related to the most promising MOF solids with decorated amino functional groups. The thermogravimetric curves of I_2@UiO-n samples have been considered between room temperature and a first plateau, corresponding to a weight loss assigned to the removal of gaseous iodine encapsulated within the pores. The related plateau was defined by a temperature value, estimated at the intersection of the tangents of the weight losses attributed to iodine and the starting departure of organic linkers. As shown in Figure S91, an illustration is given for the thermogravimetric curve occurring for I_2@UiO-66_NH_2, which indicates a desorption process of iodine between room temperature up to 280°C. All the release temperature values have been measured in a similar manner (Figure S92) and listed in the Table from Figure 4.

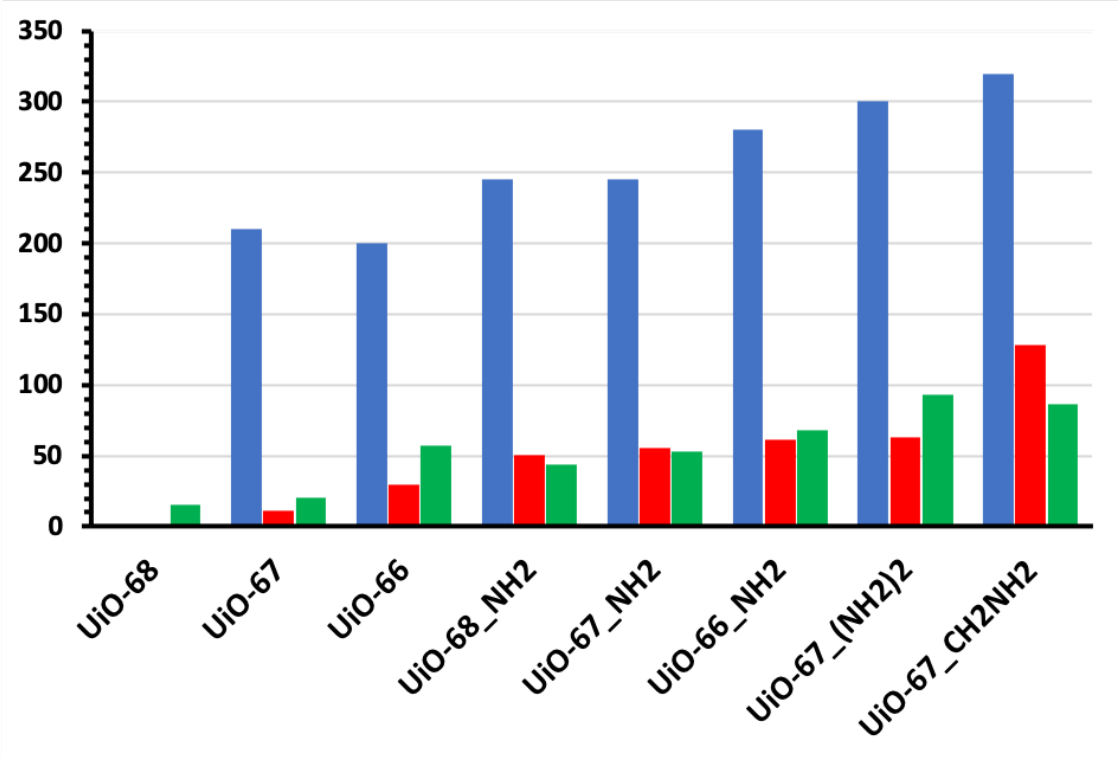

	UiO-68	UiO-67	UiO-66	UiO-68 _NH_2	UiO-67 _NH_2	UiO-66 _NH_2	UiO-67 _$(NH_2)_2$	UiO-67 _CH_2NH_2
Iodine release temperature (°C) (TGA)	n.m.*	210	200	245	245	280	300	320
ΔE_{int} I_2 OCTA cage (kJ.mol^{-1})	-1.6	-11.3	-29.9	-50.3	-55.3	-61.6	-63.2	-128.5
ΔE_{disp} OCTA cage (kJ.mol^{-1})	-2.3	-10.7	-24.9	-21.5	-25.6	-35.1	-20.1	-38.5
ΔE_{int} I_2 TETRA cage (kJ.mol^{-1})	-15.9	-20.7	-57.1	-43.9	-53.2	-68.1	-93.4	-86.7
ΔE_{disp} TETRA cage (kJ.mol^{-1})	-13.7	-17.8	-48.3	-21.9	-31.3	-37.1	-29.3	-41.1

*n.m.: not measured.

Figure 4. Comparison of the maximal iodine release temperature (blue bars) with the theoretical interaction energies values between molecular iodine and organic linkers in different I_2@UiO-n compounds. Red and green bars indicate absolute interaction energies ($-\Delta E_{int}$) in OCTA and TETRA cavities, respectively.

Table: first raw and blue bar: maximal temperature of iodine release from I_2@UiO-n samples, estimated by thermogravimetric analysis. Second and fourth raws (grey): calculated interaction energies (ΔE_{int}) for one molecule of I_2 located either in octahedral (OCTA) or tetrahedral (TETRA) cavity of UiO-n network. Third and fifth raws:

contribution of dispersion interactions (ΔE_{disp}) for I_2 located either in octahedral (OCTA) or tetrahedral (TETRA) cavity of UiO-n network.

The iodine release temperatures are almost identical for the UIO-66/UiO-67 frameworks (200 and 210°C, respectively), with no amino functional group. These values are higher than the sublimation temperature of iodine (184°C) under atmospheric pressure, confirming a relative affinity of iodine with the aromatic linker. The amino-decorated UiO-66/UiO-67/UiO-68 samples are characterized by higher release temperature of iodine. The compounds I_2@UiO-67_NH_2 and I_2@UiO-68_NH_2 possess the same release temperature at 245°C, but its analog with shorter ditopic linker has a higher temperature value at 280°C, which can be attributed to the confinement effect due to smaller pore size in UiO-66_NH_2. The retention of iodine is improved if the amino content increases, as illustrated for the UiO-67_$(NH_2)_2$, with a temperature of 300°C. At last, the best temperature is observed for the UiO-67_CH_2NH_2 with a value of 320°C.

From thermogravimetric analyzes, we have thus shown differentiated interactions of iodine with the different frameworks of UiO-n (Zr) bearing various decoration of amino functional groups. In order to quantify these interactions, we tentatively estimated their energies between molecular iodine and organic linkers, depending on their location on the large cavities (octahedral – OCTA) or small cavities (tetrahedral – TETRA) of the UiO-n topology. The modeling results are summarized in the table of Figure 4, and correspond to a series of UiO-n studied experimentally in the present work, as well as the pristine UiO-68.

Using equations (1) and (2), calculated interaction energies of I_2 with the corresponding contributions of the dispersion forces for all the UiO-n series are reported in the table of figure 4. As it can be seen, the computed interaction energies (ΔE_{int}) of I_2 range from -1.6 kJ.mol^{-1} (UiO-68) to -128.5 kJ.mol^{-1} (UiO-67_CH_2NH_2), depending on the UiO-n structures and the adsorption sites (OCTA or TETRA). Analyzing (ΔE_{int}) of I_2 obtained with the non-modified UiO series (UiO-66, UiO-67 and UiO-68), an important energy difference between the octahedral and tetrahedral sites are observed. For example, the computed ΔE_{int} (TETRA) - ΔE_{int} (OCTA) difference for UiO-66 is 27.2 kJ.mol^{-1} due to the evolution of the pore size which influences the dispersion interactions. Nevertheless, for these UiO-n structures, the computed interaction energies of I_2 are low and do not exceed -57 kJ.mol^{-1}. This value is comparable to the interaction energy computed in the pyrene-based Metal-Organic Framework SION-8, [53] or in related materials, including the UiO-n series.[54] The highest absolute value of interaction energies of I_2 is obtained with UiO-66 followed in order by UiO-67 and UiO-68. This can be explained by the increase of the organic linkers lenghts, which involves larger pore apertures that reduce the interaction between I_2 and the UiO-n structures. For UiO-68, the ΔE_{int} of I_2 are practically equal to zero (-1.6 kJ.mol^{-1}, OCTA cavity). Furthermore, for the non-substituted UiO compounds, the interaction of iodine with organic linkers is dominated by dispersion interactions (more than 60% of the total interaction energy). The present results are in line with our recent work which showed that the long-range non-bonding of iodine and RuO_4 species with different MOF compounds (MIL-53 (Al), MIL-120 (Al) and HKUST-1 (Cu)) are very important.[43,55] Let us now turn to the impact of the amino functionalization. Following the results obtained in Sections 3.1 & 3.2, the functionalization of the organic linkers in UiO-66, UiO-67 and UiO-68 with –NH_2 groups, appears as an efficient adsorbent to trap iodine. To

further elucidate the roles of $–NH_2$ into the UiO-n series, calculated interaction energies of I_2 were investigated at the molecular level with UiO-66_NH_2, UiO-67_NH_2 and UiO-68_NH_2 (Table in figure 4). In that case, we have replaced one hydrogen atom by $–NH_2$ group in the ortho position (Figure 1). For UiO-66_NH_2, UiO-67_NH_2 and UiO-68_NH_2, slightest differences in the interaction energy are observed between the three selected structures since ΔE_{int} of I_2 spread into a small interval of values (from -43 to -68 kJ.mol^{-1}). In addition, it is clear from Figure 4 that the ΔE_{int} of I_2 are quite similar for both octahedral and tetrahedral sites for all the UiO-n structures. This is due to the direct interaction between I atom (I_2) and $–NH_2$ lone pair of the group attached to the organic ligand. The addition of a second $–NH_2$ group on the ditopic organic linker in UiO-67 framework led to enhanced values of interaction energies (ΔE_{int}) for I_2, for both OCTA cavities (from -55.3 [UiO-67_NH_2] to -63.2 kJ.mol^{-1}[UiO-67_$(NH_2)_2$]) and TETRA cavities (from -53.2 [UiO-67_NH_2] to -93.4 kJ.mol^{-1}[UiO-67_$(NH_2)_2$]), with a larger gap for the TETRA one. Indeed, the latter value is the highest one for this series for the TETRA cage.

Beyond these interesting results, to further improve significantly the capture of I_2, we tested aliphatic amines, for which the nitrogen lone pair is not conjugated with the aromatic group and is more available to interact with the iodine. In this purpose, we have assessed the impact of replacing $–NH_2$ group by $–CH_2NH_2$ on UiO-67 (Figure 4). Herein, considerable increase of the interaction energy of I_2 is observed compared to the results obtained with UiO-67_NH_2 and UiO-67 structures. The ΔE_{int} of I_2 are -86.7 and -128.5 kJ.mol^{-1} in tetrahedral and octahedral cavities of UiO-67_CH_2NH_2, respectively. The dispersion energy contribution to this quantity is relatively lower: -41.1 and -38.5 kJ.mol^{-1} for tetrahedral and octahedral cavities, respectively. The very important role of the nitrogen lone pair can be illustrated through the representation of the electronic density difference ($\Delta\rho$) induced by the adsorption (Figure 5). As expected, for UiO-67 structure, there is almost no electron transfer between the framework and I_2, in the line with the very low interaction energy (-11.3 kJ.mol^{-1}). In the case of UiO-67_NH_2 (ΔE_{int} of I_2 is -55.3 kJ.mol^{-1}), we can find an important electron exchange between iodine and the $–NH_2$ group but also with the aromatic cycle. Importantly, in the case of UiO-67_CH_2NH_2, we underline a significant electron transfer between $-CH_2NH_2$ group and iodine, hence the highest calculated interaction energy of I_2 (-128.5 kJ.mol^{-1}). The success of UiO-67_CH_2NH_2 made that structure as one of the most efficient adsorbents in iodine immobilization.

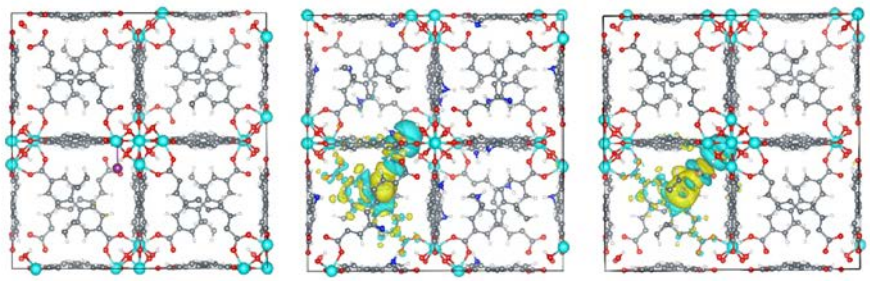

Figure 5. Difference in electronic density for UiO-67 (left), UiO-67_NH_2 (middle) and UiO-67_CH_2NH_2. The blue (yellow) zones indicate density decrease (increase). Color code: O atoms are in red, C atoms in grey, Zr atoms in sky blue, N atoms in blue and H atoms in white.

The comparison of these theoretical calculations and the experimental values resulting from the thermogravimetric analyzes, shows a good correlation (Figure 5). The highest interaction energy is related to the highest iodine release temperature in the UiO-n series (320°C), confirming the significant role of the interaction between -NH_2 lone pair (especially when attached to an aliphatic fragment) and the I_2 molecule.

3.4 Preliminary UV-Vis spectroscopy analyzes of I_2@UiO-66 and I_2@UiO-66_NH_2 compounds.

Spectroscopic analyses have been carried out for a selection of two UiO-n materials, related to the UiO-66 compound and its amino-functionalized derivative, UiO-66_NH_2. A first eye-observation shows that the powdered sample of pristine UiO-66 is white, whereas the UiO-66_NH_2 solid exhibits a pale yellowish color. The iodine loading process turns pink color for these two samples, as usually observed for this type of iodine-loaded MOF compounds.[17,56] However, when stored in a closed glass cell in daylight, its color turns into orange/brown after less than one hour (Figure 6). However, when the iodine-loaded compound I_2@UiO-66 is stored in darkness, its pink color does not change. A photochemical process can be therefore assumed in order to understand these color variations over time, depending on the storage conditions (light/dark). This color modification can be attributed to a chemical transformation of the initial gaseous molecular iodine, which could undergo a redox process.

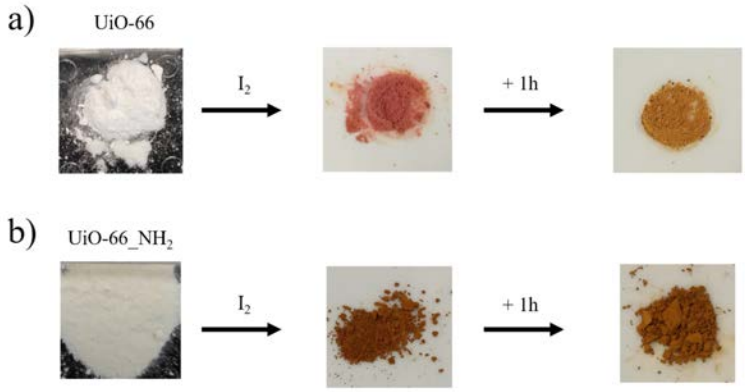

Figure 6. Eye-optical evolution of UiO-66 and UiO-66_NH_2 colors, from original powdered samples (left), then after iodine loading for 16h (middle), followed by storing in glass cell for 1 h (right). The color of samples kept in darkness, does not change, after storing.

This initial color modification incited us to further characterize these two compounds by UV-Vis spectroscopy. Before iodine loading, the UV-Vis spectrum of UiO-66 compound shows bands characteristic of the MOF at 230 nm and located at around 275 nm (Figure 7a), which is usually attributed to the charge transfer process between one metal and an organic linker.[57] An UV-Vis spectrum has been collected for a I_2@UiO-66 sample after iodine loading 16 h (corresponding to iodine uptake of 181 $mg.g^{-1}$ or 1.19 $I_2.mol^{-1}$), followed by 30 minutes in glass cell under daylight (time required for the transfer of the sample from the iodine sorption setup to the UV-Vis spectrometer). A second broad band at 390 nm appears and is assigned to a charge transfer between iodine and the aromatic ring of the terephthalate occurring in UiO-66 framework, as previously described in a mixed solution of hexamethylbenzene-iodine[58] or in MOF-like materials.[17,59] In the case of non-perturbed iodine, a prominent band should be

visible in the range 450-550 nm, depending on the nature of inert organic molecule or solvent. [60,61] The UV-Vis spectrum of I_2@UiO-66 sample collected after 24 h storing under daylight, clearly shows an evolution with the presence of bands at 290 and 361 nm. This signature reveals the formation occurrence of an anionic species I_3^-, with such a typical doublet.[62] This specific moiety can be produced under light excitation of a tetrabutylammonium iodide salt in acetonitrile.[62,63]

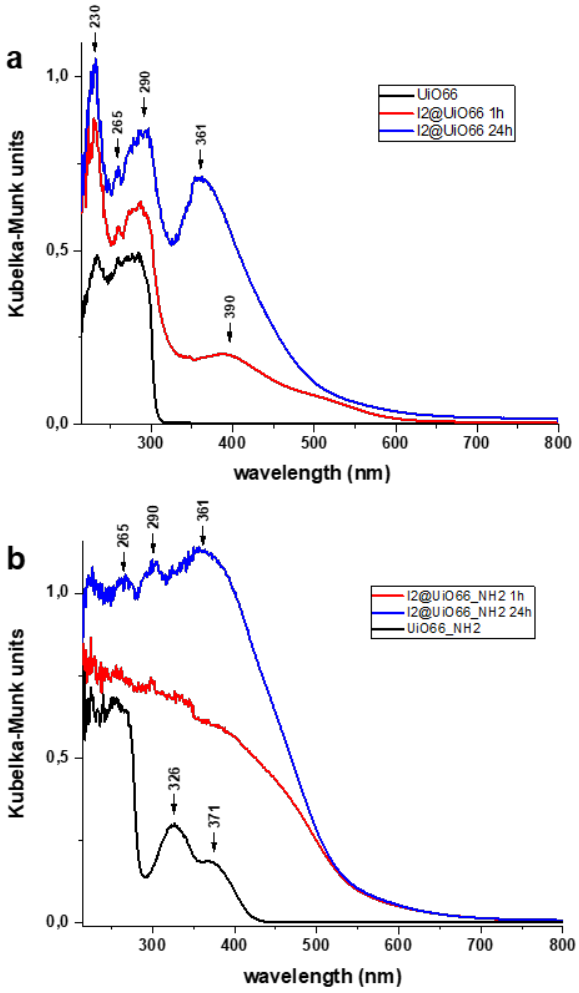

Figure 7. Diffuse reflectance UV-Vis spectra for a) UiO-66 and b) UiO-66_NH_2, before iodine loading (black line), after 16h iodine loading, followed by 30 min storing (red line), and then after 24h storing in daylight (blue line).

The UV-Vis spectrum of UiO-66_NH_2 also shows at around 265 nm (Figure 7b), a band related to the ligand to metal charge transfer complex[57] but we observe two additional bands at 326 and 371 nm, due to the presence of amino functional group.[64,65] The UV-Vis spectrum of I_2@UiO-66_NH_2 (iodine loading for 16h, corresponding to iodine uptake of 449 $mg.g^{-1}$ (or 3.10 $I_2.mol^{-1}$) collected after 30 min, does not exhibit any resolved bands, with a very broad component between 300 and 500 nm. However, after 24 h storage, the spectrum reveals the bands at 290 and 361nm, but less intense, compared to those observed in the previous sample, I_2@UiO-66, and related to the occurrence of the I_3^- species, which corresponds to as complex formed between I_2 and I^-.

The redox $I_2 \rightarrow I_3^-$ conversion was unexpected in our system and was observed in a few previous studies,[24] but was not mentioned in other works.[22,26] This reaction will be further characterized by Raman and EPR spectroscopies.

3.5 Raman spectroscopy analysis of I_2@UiO-66, I_2@UiO-66_NH_2 and UiO-67 derivatives compounds.

The Raman spectroscopy characterization have been performed for the UiO-66 and UiO-66_NH_2 compounds. The evolution of iodine species has been investigated for two arbitrarily iodine loadings set at 1 h and 16 h. They correspond to the iodine uptake of 74 $mg.g^{-1}$ (0.48 $I_2.mol^{-1}$ of UiO-66) and 72 $mg.g^{-1}$ (0.50 $I_2.mol^{-1}$ of UiO-66_NH_2) for 1 h, and 181 $mg.g^{-1}$ (1.19 $I_2.mol^{-1}$ of UiO-66) and 449 $mg.g^{-1}$ (3.10 $I_2.mol^{-1}$ of UiO-66_NH_2) for 16 h.

The FT-Raman spectra have been recorded between 50 and 3600 cm^{-1} for all samples and the reference spectra of the iodine-free MOF, either UiO-66 or UiO-66_NH_2, are shown for comparison in all series (Figures 8, 9 and S101; spectrum a). After iodine sorption, four series of Raman spectra have been collected with various storing times in daylight conditions corresponding to I_2@UiO-66 (1 h and 16 h I_2 loading) and I_2@UiO-66_NH_2 (1 h and 16 h I_2 loading) samples placed in closed quartz cell: + 10 min, just after iodine sorption, removed from sorption setup (spectrum b); after 2 hours storing (spectrum c); after 24 h storing (spectrum d); after 1 week storing spectrum e).

The Raman bands of the UiO-66_X (X = H or NH_2) compounds are essentially characteristic of the organic contribution to the structure due to the terephthalate linker at 1617, 1450, 1431, 1143 and 862 cm^{-1} for UiO-66 and at 1623, 1591, 1446, 1426, 1275, 1235 and 800 cm^{-1} for UiO-66_NH_2.[66] Figure 8A shows the Raman spectra obtained as a function of time over the range 50-1800 cm^{-1} after high loading of I_2 (16 h) on I_2@UiO-66. These spectra are representative of the behaviors observed for other samples which are presented with this spectral range in the Supporting Information file (Figure S101). It is worth noting that the porous network bands keep the same positions and relative intensities as a function of storing time upon I_2 adsorption and conversion to subsequent species such as I_3^-. This feature reveals that the iodine encapsulation does not alter the topology of the UiO-n materials. Nevertheless, after seven days of storing, slight shifts and relative intensity changes can be observed in the 1200-1600 cm^{-1} region due to stronger interaction between iodine species and the UiO-n structure.

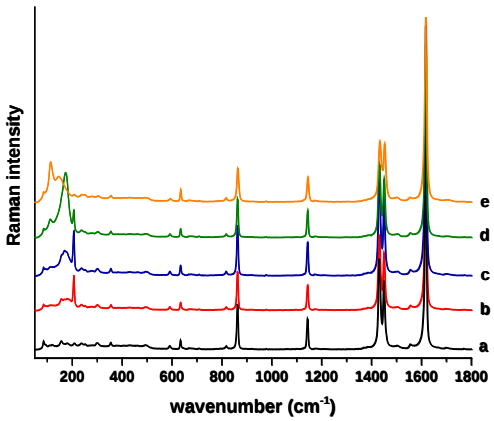

Figure 8. Time evolution of the Raman spectra of the I_2@UiO-66 compounds in the 50-1800 cm^{-1} range after 16h iodine loading with different daylight storing times (b: + 10 min; c + 2 h; d: + 24 h; e: + 1 week). Spectrum a corresponds to the pristine UiO-66 sample before iodine loading.

The characteristic Raman bands related to the iodine species are typically observed in the range 50-250 cm^{-1} and presented in Figure 9. All the I_2@UiO-66 and I_2@UiO-66_NH_2 spectra have been compared from the benchmarking iodine unloading sample, normalized with the bands at 1617 cm^{-1} (for UiO-66) and at 1623 cm^{-1} (for UiO-66_NH_2) with a constant intensity whatever the iodine content or reaction time, and assigned to the UiO-66 network. This operation allowed us to compare the evolution of Raman peak intensities, to access to the relative concentration changes of the different iodine species observed in our study.

After 1 h iodine loading (Figure 9A, spectrum b), the Raman spectrum of UiO-66 (t = 10 min) shows a dominant single narrow band at 206 cm^{-1}, which is typical of the I-I stretching of a "free" molecular I_2 moiety, revealing a weak interaction between iodine and organic linkers. This value is closely related to that of benzene-I_2 complexes.[67,68] After 2 h (Figure 9A, spectrum c), the 206 cm^{-1} stretching mode intensity decreases together with the enhance of a group of three broader peaks located at 180, 169 and 157 cm^{-1}. These values are lower than that observed in the crystalline I_2 solid (180-188 cm^{-1}).[69] These three components range are usually related to molecular iodine in strong interaction with organic donor molecules,[67] which induces the decreasing of the frequency. They are assigned to "perturbed" iodine through charge transfer complex process,[59] which may result in the generation of multitude of anionic polynuclear iodides species of I_n^- type (n = 3, 5, 7 …). Moreover, it was reported that the observation of the intra-molecular I-I distance lengthening could be correlated to the frequency decrease, in some thioketone adducts products.[70] The Raman spectrum collected after 24 h (Figure 9A, spectrum d) exhibits the same evolution peak, with the significant intensities increasing in the 180-157 cm^{-1} region (two resolved peaks at 169 and 157 cm^{-1} and weaker shoulder at 178 cm^{-1}, against the slow decrease of the original band intensity at 206 cm^{-1}. However, a new vibration band appears at around 114 cm^{-1}, and is definitely the signature of the anionic species I_3^-.[70–73] After 1 week (Figure 9A, spectrum e), the Raman spectrum only shows the large band at 114 cm^{-1} together with a second weaker component at around 140 cm^{-1}, which are both attributed to the species I_3^-. Indeed, these two bands are typical of the symmetric and asymmetric stretching vibrations of the anion I_3^-, respectively.[74–76] The observation of these two peaks rules out the occurrence of I_2^- anion, since only the component at 114 cm^{-1} is present for the latter.[77]

Nevertheless, literature also described the occurrence of this range of vibrations, related to anionic complexes I_3^- corresponding to the species $I^-\cdots I_2$, or I_5^-, with two distinct combinations ($I_2\cdots I^-\cdots I_2$ or $I_3^-\cdots I_2$). In general, higher nuclearities of anionic iodide species involve vibration bands in higher frequencies (up to 161 cm^{-1} for I_5^- [75] and 175 cm^{-1} for I_5^- [76] or I_7^- , for instance).[34]

Despite the complexity of encapsulated iodide anions within MOF pores, the existence of I_3^-, illustrated by the two typical components at 140 and 114 cm^{-1}, is the most currently reported and will be used in our present study.[59,78] For the UiO-66 spectrum e (1 h loading time; Figure 9A), the components of the "free" iodine and "perturbed" iodine through charge transfer complex have disappeared.

The second compound UiO-66 analyzed with a higher iodine loading (16 h; Figure 9B), exhibits a similar variation of the vibration bands intensities, with some differences. Whereas the band at 206 cm^{-1} is present for short storage durations (+10 min / + 2h), the appearance of the component in the 178-157 cm^{-1} region is not so well resolved, since only a broad peak emerges, centered at around 173 cm^{-1} in the spectrum d (+ 24 h; Figure 9B), attributed to the iodine involved in charge transfer complex. After 1 week, an identical Raman spectrum is observed with only the components at 145 cm^{-1} (medium intensity) and 114 cm^{-1} (high intensity) typically related to the I_3^-. This time evolution reveals that a redox chemical reaction with the $I_2 \rightarrow I_3^-$ conversion slowly occurs when molecular iodine is encapsulated within pore system of the UiO-66 material, as suggested by our previous UV-Vis spectroscopic study. It is noteworthy that such host-guest charge transfer with iodine-iodide transformation sequence, was described in MOF materials by either partial oxidation of vanadium(III) centers[79] or applying high pressure (up to 8.4 GPa).[59]

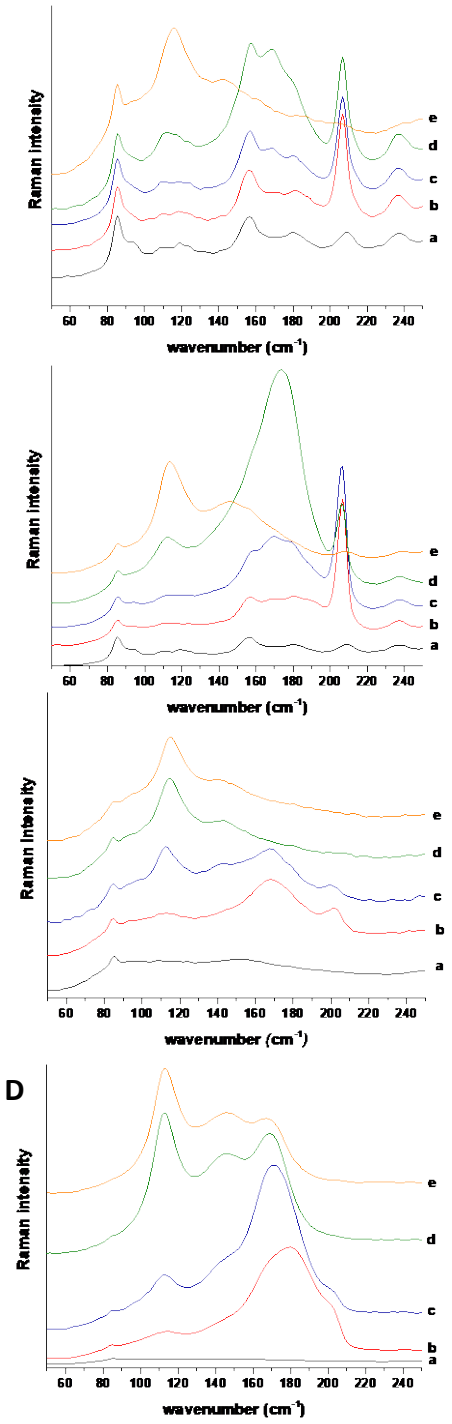

Figure 9. Time evolution of the Raman spectra of the I_2@UiO-66 and I_2@UiO-66_NH_2 compounds in the 50-250 cm^{-1} range after iodine loading with different daylight storing times (b: + 10 min; c + 2 h; d: + 24 h; e: + 1 week). Spectrum a corresponds to the pristine UiO-66 or UiO-66_NH_2 sample before iodine loading. From top to bottom: A: I_2@UiO-66 after 1 h iodine loading. B: I_2@UiO-66 after 16 h loading. C: I_2@UiO-66_NH_2 after 1 h iodine loading. D: I_2@UiO-66_NH_2 after 16 h iodine loading. Normalization was carried tout using the 1617 cm^{-1} band of UiO-66 and the 1623 cm^{-1} band of UiO-66_NH_2, respectively.

The similar collection of Raman spectra has been carried out for the UiO-66_NH_2 compounds (Figures 9C and 9D). The global time evolution of the Raman spectra is close to those observed with the first series of UiO-66 (Figures 9A and 9B), with the first disappearance of the initial

vibration band of molecular "free" I_2 (in this case at 202 cm^{-1}), followed by the growing of broad band at around 180-160 cm^{-1}, related to "perturbed" iodine from charge transfer complex, and then the observation of specific bands at 140 or 145 cm^{-1} and 114 cm^{-1}, assigned to the anionic I_3^- species. However, the kinetic of formation of these successive iodine/iodide moieties sequence is faster, when the amino functional group is present in the UiO-66_NH_2 framework. Indeed, the original band at 202 cm^{-1} is rather weak, from the starting experience (spectrum b, t = 10 min) and is absent after 24 h (spectrum d; Figure 9C). It is noticed that the shift (from 206 cm^{-1} in UiO-66 $\rightarrow$ 202 cm^{-1}) may indicate a slightly stronger interaction of molecular I_2 in UiO-66_NH_2. Correlatively, the broad component in the region 180-160 cm^{-1} is immediately visible as intense band, from short storage time (+10 min). These two features (low concentration of "free" molecular I_2 + charge transfer "perturbed" complex) are specifically due to the amino groups which favor the rapid interaction of iodine with the UiO-66_NH_2 framework. The conversion into I_3^- is thus faster, since it starts appearing from the spectrum b (t =10 min; Figure 9C), but is more effective after 2 h (spectrum c; Figure 9C), whereas the I_3^- species were only observed for the spectrum d (after 24 h; Figure 9C). Moreover, for the compound UiO-66_NH_2, the signature of iodine involved in charge transfer complex moves from 181 cm^{-1} at t = 10 min, to 169 cm^{-1} from t = 2 h, which is related to stronger charge transfer complex effect with increasing time. Due to higher iodine loading in UiO-66_NH_2 (3.10 $I_2.mol^{-1}$, instead of 1.19 $I_2.mol^{-1}$ of UiO-66, after 16 h sorption), the component of the "perturbed" iodine with charge transfer complex is still present together with I_3^-, whereas only the latter anionic species occurred for low iodine loading (i.e $\approx$0.5 or 1.19 $I_2.mol^{-1}$ in UiO-66 or UiO-66_NH_2, respectively; see Figure 9A or 9C, spectra e). Therefore, this observation seems to indicate that the conversion of the redox chemical process $I_2 \rightarrow I_3^-$ is limited if the iodine concentration is too high within the network pores, at a given time (here, after one week).

In order to highlight the effect of the presence of amino groups on the evolution of iodine species, the intensities of the Raman bands at 206 cm^{-1} (free iodine), 170 cm^{-1} (perturbed iodine) and 114 cm^{-1} (I_3^-) were plotted as a function of time just after the iodine loading uptake of 1 hour (Figure 10).

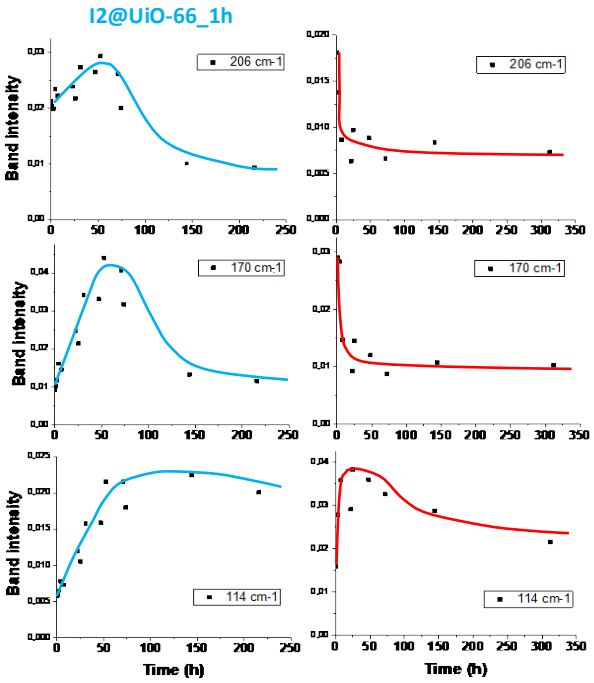

Figure 10. Evolution as a function of time of the intensities of the 206, 170 and 114 cm^{-1} Raman bands after low I_2 loading (1 h) on UiO-66 (left) and UiO-66_NH_2 (right).

For I_2@UiO-66 and 1 h iodine loading, the time evolution graphs show three different behaviors depending on the iodine species. The 206 cm^{-1} band intensity is nearly already on a plateau at the beginning and decreases progressively from about 60 h. The intensity of the band at 170 cm^{-1} increases to a maximum after about 75 h and then gradually decreases to a very low intensity after 7 days (168 h). The intensity of the 114 cm^{-1} band also increases gradually to reach a maximum after about 75 h, and then remains stable for periods longer than a week.
For I_2@UiO-66_NH_2, the I_3^- band at 114 cm^{-1} also increases to reach a maximum after about 10 h and slightly decreases for a duration longer than seven days. In contrast to what is observed for I_2@UiO-66, the 170 and 206 cm^{-1} bands decrease continuously from the first spectrum recorded at the end of the loading period for I_2@UiO-66_NH_2. Thus, the comparison of these two samples clearly shows the dramatic increase in the kinetics of iodine adsorption and conversion to I_3^- in the presence of the amino group.
It is worth noting that identical behavior is observed for the evolution of I_2@UiO-66 and I_2@UiO-66_NH_2 samples in terms of species evolution after a 16 h iodine loading period. However, the kinetics of formation and disappearance of iodine species is much faster (figure S102). Furthermore, it is interesting to note that the perturbed iodine at 170 cm^{-1} is still clearly present after 1 week, in the presence of the amino group whereas this species is very weak for the same period of time in the case of 1 h iodine loading and without amino group; this could be due to the fact that the amount of "perturbed I_2" is too high to fully react with I^- to form I_3^-.
The histograms presented in Figure 11 depict the Raman intensity of the band corresponding to the symmetric stretching of I_3^- at 114 cm^{-1} normalized with the bands at 1617 cm^{-1} (UiO-66) and 1623 cm^{-1} (UiO-66_NH_2) after 7 days and compare the effects of NH_2 group and of loading time. It is clear that increasing the loading time of I_2 from 1 h to 16 h increases the amounts of I_3^- for both I_2@UiO-66 and I_2@UiO-66_NH_2. But if the increase is moderate with I_2@UiO-66, it is much more significant in the presence of amino groups. At the opposite, when considering

the kinetics of I_3^- formation (Figures 10 and S102), we also observe that, after several days (> 3-7 days), the intensity of the I_3^- signal at 114 cm^{-1}, decreases significantly, particularly for the amino-functionalized UiO-66_NH_2 compound. This behavior might be due to the slow desorption of iodide species from the UiO-n framework, which occurs for high iodine contents, due to the presence of amino groups. This behavior is thus enhanced for the highest iodine loading in UiO-66_NH_2: at 1 h I_2 loading, intensity of I_3^- signal decreased by a factor of ≈1.5 after 14 days; at 16 h I_2 loading, intensity of I_3^- signal decreased by a factor of ≈3 after 33 days)

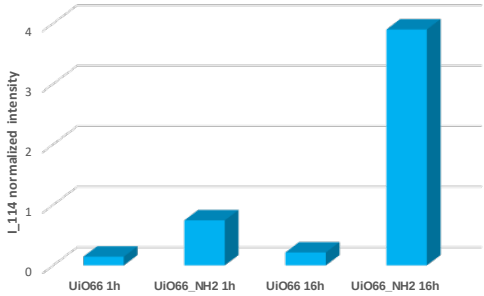

Figure 11. Raman intensity of the band corresponding to the symmetric stretching of I_3^- at 114 cm^{-1} normalized with the bands at 1617 cm^{-1} (UiO-66) or 1623 cm^{-1} (UiO-66_NH_2) after 7 days storing time.

Experiments carried out with UiO-67 and UiO-67_NH_2 after high I_2 loading (16 h) show the same trend (Figures S103A and S103B). The presence of the amino group indeed leads to an increase in the amount of I_2 adsorbed but the stabilized iodine species on UiO-67 after seven days is only I_3^- (114 cm^{-1}) whereas the contributions of I_3^- and perturbed I_2 (170 cm^{-1}) show similar intensities. This excess of I_2 adsorbed on the surface of UiO-67_NH_2 seems to be the limiting or slowing down factor for I_3^- formation as suggested above after the capture of I_2 by UiO-66 with and without NH_2 group.

In addition, comparison is made between four samples that belong to the UiO-67 series with the H (UiO-67), NH_2 (UiO-67_NH_2), $(NH_2)_2$ (UiO-67_$(NH_2)_2$) and CH_2NH_2 (UiO-67_CH_2NH_2) functionalization. The spectra show the same trend and the stabilization of I_3^- species after 7 days (Figures S103C and S103D). However, significant differences are observed in the absorption kinetics. Indeed, iodine uptake is much faster when UiO-67 is functionalized with $(NH_2)_2$ and CH_2NH_2 groups. In particular, the spectral signature of I_3^- is already very intense after 2 h for UiO-67_CH_2NH_2, for which the "perturbed I_2" band at about 170 cm^{-1} remains very weak. This result is related to the kinetic curve of adsorption of iodine gas in UiO-67 derived compounds at room temperature presented above in Figure 3 since the $(-NH_2)_2$ and especially $-CH_2NH_2$ groups seem to accelerate considerably the adsorption process in the first steps of the adsorption reaction.

Finally, the same trend is observed for I_2@UiO68_NH_2 for which I_3^- is clearly the stabilized species after 7 days (Figure S103E).

In order to tentatively elucidate the active intermediates occurring during the mechanism of the iodine conversion into anionic I_3^--like species within the UiO-66 framework, we investigated the samples I_2@UiO-66 and I_2@UiO-66_NH_2 by Electron Paramagnetic Resonance (EPR) spectroscopy. Without any observation of signal attributed to the occurrence of Zr^{3+} species, we

concluded that the zirconium metallic center is not involved in the $I_2 \rightarrow I_3^-$ conversion (see supporting Info S11).

3.6 Raman spectroscopy mapping.

In a second part, we investigated the spatial distribution of iodine species from a single-crystal of UiO-67_NH_2 after iodine sorption experiment for 16 h. This specific UiO-n sample has been selected due to its easy crystal growth, generating large single-crystal of around 50 μm size with typical well-shaped octahedra. These dimensions are suitable for an observation under the binocular optical microscope equipped on our Raman spectrometer (Horiba Scientific). We noted the occurrence of holes of few μm at the surface of triangular faces of octahedra, indicating the presence of crystal growth defects (Figure 12).

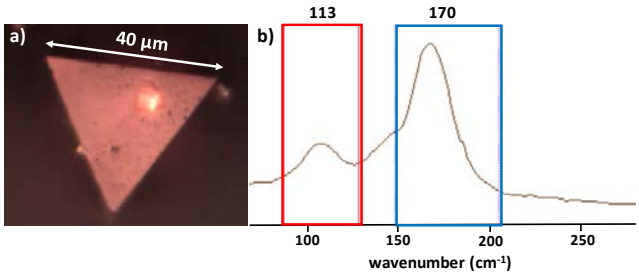

Figure 12. a) photograph showing the triangular face of the octahedral-shaped single-crystal of UiO-67_NH_2. b): Raman spectrum showing the two main bands centered at 170 cm^{-1} ("perturbed" I_2) and 113 cm^{-1} (anionic I_3^-), which have been considered for the iodine mapping.

The observed intensities of the Raman bands are therefore representative of the relative spectral concentration of the iodine species in the single-crystal. The Figure 13 shows the maps obtained for the UiO-67_NH_2 crystal presented in Figure 12a, with the upper triangular face of 40 μm size. The maps are represented with a color change. These colors represent the intensities of the selected bands, chosen arbitrarily and represented in scales to the rights of the maps.

The Raman spectra are all characterized by two main vibration bands, centered around 170 and 113 cm^{-1}, assigned to the "perturbed" I_2 involved in charge transfer complex and anionic I_3^- species, respectively (Figure 12b). It is interesting to note that the band intensity ratio I(170)/I(113) obtained here using the 633 nm laser excitation is identical to that obtained using FT-Raman using the 1064 nm excitation line for a similar time. This result reflects the absence of Raman resonance enhancement in both cases and indicates that the intensity ratio is proportional to the species concentration.

The first series of maps (Figure 13) shows the distribution of the adsorbed I_2 species (170 cm^{-1}) at the surface and over a depth varying from 0 to 12 μm. At the surface (0-2 μm), the "perturbed" iodine species seems to appear slightly more intense on the left side of the crystal. This trend is confirmed by in-depth analysis where the iodine concentration clearly appears stronger on the left side (6 μm). After contact with the surface of UiO-67_NH_2 and adsorption, the iodine diffusion seems to proceed gradually from the left to the center of the crystal. In addition, the images show that the cavity on the surface of the crystal is a stopping point for the adsorption and diffusion of iodine. Focusing the laser beam at 12 μm makes it possible to highlight the octahedral shape of the crystal by observing a signal at the periphery. The intensity

decrease observed for the in-depth analyses may indicate a lower iodine concentration, but also be linked to the lower excitation light intensity at the focal point, after having passed through the crystal and therefore to a lower number of scattered photons.

The maps (Figure 13) obtained for I_3^- species (113 cm^{-1}) show exactly the same trends as those described above for adsorbed iodine with diffusion from left to right. This result is consistent since the areas richest in adsorbed iodine must lead to the stronger conversion to I_3^-. The intensity of the lines at 113 cm^{-1} nevertheless appears weaker than that located at 170 cm^{-1}, and seems to indicated that I_2 remains predominant. However, it should be remembered that the Raman intensity depends on the scattering cross sections of the species and therefore on their geometry. Consequently, due to the various possible forms of I_3^-, even $I_3^-\cdots I_2$ and of I_2 adsorbed in interaction with the surface, the geometry of these iodine species is not known with accuracy, and it is not possible to determine the concentrations in the absence of prior calibration.

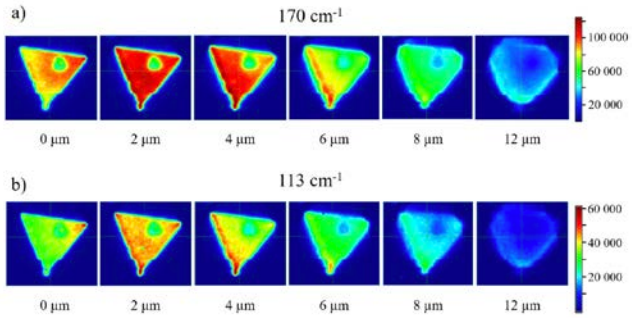

Figure 13. Raman mappings related to the areas of peaks at 170 cm^{-1} (top) and 113 cm^{-1} of the I_2@UiO-67_NH_2 compound, after 16 h iodine loading, as a function of single-crystal depth (0-12 µm). On right, color scale is related to the arbitrarily intensity of a given frequency (either at 170 or 113 cm^{-1}).

4. CONCLUSION

This work described the influence of the functionalization of zirconium-based UiO-n MOF-type materials, with different organic groups (-H, -CH_3, -Cl, -Br, -$(OH)_2$, -NO_2, -NH_2, -CH_2NH_2) for their gaseous iodine adsorption. For this purpose, we designed a home-made setup for the dynamic measurement of the iodine uptake, since previous works mainly reported the adsorption of gaseous iodine in MOF solids in batch experiments. Kinetic curves of iodine sorption have thus been measured up to 48 hours and showed the drastic effect of amino functionalization. Indeed, iodine uptakes of 210 and 222 $mg.g^{-1}$ have been observed for the pristine UiO-66 and UiO-67, respectively. Our study emphasized the drastic role of the functionalization of the benzene ring from the organic ligands as ditopic spacer between the hexanuclear {$Zr_6O_4(OH)_4$} building units. In fact, it was observed that the occurrence of amino groups (-NH_2) improved the iodine adsorption capacity by a factor up to 2.7 in the UiO-66 series (for UiO-66_NH_2; 565 $mg.g^{-1}$) and up to 5.5 in the UiO-67 series (for UiO-67_$(NH_2)_2$; 1211 $mg.g^{-1}$). However, the increasing length of the ditopic ligand has a reverse impact since the cavity aperture is too much large when comparing with the iodine diameter, in UiO-68_NH_2 compounds (300 $mg.g^{-1}$).

We also explored for the first time, the effect of attached alkylamine function in MOF solids, by considering the -CH_2NH_2 group, instead of -NH_2, in the particular case of UiO-67. Indeed, the iodine capacity was lower (660 $mg.g^{-1}$ for UiO-67_CH_2NH_2), but its interaction between

the -CH_2NH_2 group and iodine was the highest one in our UiO-n series: DFT calculations indicates interaction energies (ΔE_{int}) of I_2 value -128.5 kJ.mol^{-1} (octahedral cavity), and -86.7 kJ.mol^{-1} (tetrahedral cavity), for UiO-67_CH_2NH_2. In comparison, these values were -55.3 kJ.mol^{-1} (octahedral cavity), and -53.2 kJ.mol^{-1} (tetrahedral cavity), for UiO-67_NH_2, or -11.33 kJ.mol^{-1} (octahedral cavity) and -20.7 kJ.mol^{-1} (tetrahedral cavity) for the pristine UiO-67. It was interesting to observe a correlation of the iodine release upon temperature with these calculations, since the highest temperature of 320°C (compared with 280°C and 210°C for UiO-67_NH_2 and UiO-67, respectively) was measured for the UiO-67 showing the highest value interaction energies (ΔE_{int}) of I_2. The specific interaction of iodine was thus specifically enhanced via functional groups exhibiting lone electron pair, such as amino groups.

The chemical behavior of the trapped gaseous iodine species has been then studied in details by Raman spectroscopy, in order to characterize conversion of I_2 into I^- (stabilized as $I^-\cdots I_2$ or I_3^- complex within the pores of UiO-n materials), which occurs in time and under ambient light. Indeed, this anionic species appears with typical signatures at ≈110 and 140 cm^{-1}, and its formation kinetic is increased in the presence of the amino functionality. For instance, it is observed the $I_2 \rightarrow I_3^-$ conversion after 75 h for the pristine UiO-66 whereas it is 10 h for the UiO-66_NH_2. The Raman mapping has been performed in order to analyze the microscopic spatial distribution of trapped iodine within one single-crystal of UiO-67_NH_2. It was thus observed that a good homogeneity of both trapped I_2 species or transformed I_3^- anions through the selected crystal. At last, the EPR experiments have shown that the zirconium centers are not involved in the redox process of I_2 (no observed Zr^{3+} species). The latter seems to be rather attributable to the occurrence of O_n^- species, which are generated once I_2 molecules are inserted within the pore system of the UiO-n network.

In summary, our investigations showed the influence of the organic functionality, especially the amino groups, decorating the aromatic ring of the ditopic linkers connecting the hexanuclear brick $\{Zr_6O_4(OH)_4\}$ in UiO-n networks. A time evolution of Raman spectra clearly indicated the conversion of trapped I_2 into I^-/I_3^- in UiO-n materials, which brings new information for the capture of iodine in MOF materials. The systematic generation of anionic iodine species in this series of MOF solids, is a noticeable feature, which has to be taken into account for the strategy of investigations for finding novel solutions of molecular sieve for gaseous radioactive species in the nuclear plant accidental context. Future works will require the study of gaseous iodine capture in the presence of water and analyze its influence on the conversion of I_2 into I^-/I_3^- species when trapped within the MOF cavities.

Supporting Information. See DOI:/10.1002/chem.2021???

Organic Synthesis procedures of non-commercial organic ligands, synthesis procedures of UiO-n compounds, activation procedures, powder XRD patterns, N_2 adsorption isotherms, description of the gaseous iodine adsorption set-up, kinetic curves fittings of gaseous iodine adsorption, thermogravimetric curves, Raman spectroscopy, EPR spectroscopy (PDF).

Conflicts of interest

The authors declare no competing financial interest.

Acknowledgments

The authors would like to thank Mrs. Nora Djelal and Pr Lydie Pelinski for their assistances with the organic synthesis and thermogravimetric analyses (UCCS), and Victoria Stevenson for preliminary works about iodine capture in MOF compounds. The "Fonds Européen de Développement Régional (FEDER)", "CNRS", "Région Hauts de France" and "Ministère de l'Education Nationale de l'Enseignement Supérieur et de la Recherche" are acknowledged for the funding of X-ray diffractometers and ICP-AES apparatus from the Chevreul Institute platform. This research used resources of the Centre de Calcul de l'Université de Lille supported by the University of Lille, CPER Nord-Pas-de-Calais/FEDER, France Grille, and CNRS. Maëva Leloire thanks IRSN and Région Hauts-de-France for her PhD grant financing.

REFERENCES

[1] M. Baba, *Radiat. Meas.* **2013**, *55*, 17–21.
[2] Y.-H. Koo, Y.-S. Yang, K.-W. Song, *Prog. Nucl. Energy* **2014**, *74*, 61–70.
[3] B. J. Riley, J. D. Vienna, D. M. Strachan, J. S. McCloy, J. L. Jerden, *J. Nucl. Mater.* **2016**, *470*, 307–326.
[4] K. Jin, B. Lee, J. Park, *Coord. Chem. Rev.* **2021**, *427*, 213473.
[5] Z. Wang, Y. Huang, J. Yang, Y. Li, Q. Zhuang, J. Gu, *Dalton Trans.* **2017**, *46*, 7412–7420.
[6] C. Xiao, M. A. Silver, S. Wang, *Dalton Trans.* **2017**, *46*, 16381–16386.
[7] C. Volkringer, C. Falaise, P. Devaux, R. Giovine, V. Stevenson, F. Pourpoint, O. Lafon, M. Osmond, C. Jeanjacques, B. Marcillaud, J. C. Sabroux, T. Loiseau, *Chem. Commun.* **2016**, *52*, 12502–12505.
[8] S. L. Hanna, D. X. Rademacher, D. J. Hanson, T. Islamoglu, A. K. Olszewski, T. M. Nenoff, O. K. Farha, *Ind. Eng. Chem. Res.* **2020**, *59*, 7520–7526.
[9] S. E. Gilson, M. Fairley, P. Julien, A. G. Oliver, S. L. Hanna, G. Arntz, O. K. Farha, J. A. LaVerne, P. C. Burns, *J. Am. Chem. Soc.* **2020**, *142*, 13299–13304.
[10] A. G. Al Lafi, B. Assfour, T. Assaad, *J. Mater. Sci.* **2021**, *56*, 12154–12170.
[11] W. Yang, Q. Pan, S. Song, H. Zhang, *Inorg. Chem. Front.* **2019**, *6*, 1924–1937.
[12] D. Banerjee, C. M. Simon, S. K. Elsaidi, M. Haranczyk, P. K. Thallapally, *Chem.* **2018**, *4*, 466–494.
[13] W. Xie, D. Cui, S.-R. Zhang, Y.-H. Xu, D.-L. Jiang, *Mater. Horiz.* **2019**, *6*, 1571–1595.
[14] D. F. Sava, M. A. Rodriguez, K. W. Chapman, P. J. Chupas, J. A. Greathouse, P. S. Crozier, T. M. Nenoff, *J. Am. Chem. Soc.* **2011**, *133*, 12398–12401.
[15] K. W. Chapman, D. F. Sava, G. J. Halder, P. J. Chupas, T. M. Nenoff, *J. Am. Chem. Soc.* **2011**, *133*, 18583–18585.
[16] D. F. Sava, T. J. Garino, T. M. Nenoff, *Ind. Eng. Chem. Res.* **2012**, *51*, 614–620.
[17] C. Falaise, C. Volkringer, J. Facqueur, T. Bousquet, L. Gasnot, T. Loiseau, *Chem. Commun.* **2013**, *49*, 10320.
[18] X. Zhang, I. da Silva, H. G. W. Godfrey, S. K. Callear, S. A. Sapchenko, Y. Cheng, I. Vitórica-Yrezábal, M. D. Frogley, G. Cinque, C. C. Tang, C. Giacobbe, C. Dejoie, S. Rudić, A. J. Ramirez-Cuesta, M. A. Denecke, S. Yang, M. Schröder, *J. Am. Chem. Soc.* **2017**, *139*, 16289–16296.
[19] D. F. Sava, K. W. Chapman, M. A. Rodriguez, J. A. Greathouse, P. S. Crozier, H. Zhao, P. J. Chupas, T. M. Nenoff, *Chem. Mater.* **2013**, *25*, 2591–2596.
[20] R. J. Marshall, S. L. Griffin, C. Wilson, R. S. Forgan, *Chem. Eur. J.* **2016**, *22*, 4870–4877.
[21] M. Leloire, J. Dhainaut, P. Devaux, O. Leroy, H. Desjonqueres, S. Poirier, P. Nerisson, L. Cantrel, S. Royer, T. Loiseau, C. Volkringer, *J. Hazard. Mater.* **2021**, *416*, 125890.
[22] J. Maddock, X. Kang, L. Liu, B. Han, S. Yang, M. Schröder, *Chem.* **2021**, *3*, 525–531.
[23] M. Zahid, D. Zhang, X. Xu, M. Pan, M. H. ul haq, A. T. Reda, W. Xu, *J. Hazard. Mater.* **2021**, *416*, 125835.
[24] P. Chen, X. He, M. Pang, X. Dong, S. Zhao, W. Zhang, *ACS Appl. Mater. Interfaces* **2020**, *12*, 20429–20439.
[25] Y. Guan, Y. Li, J. Zhou, T. Zhang, J. Ding, Z. Xie, L. Wang, *Inorg. Chem.* **2021**, *60*, 9848–9856.
[26] B. Lee, J. Park, *Bull. Korean Chem. Soc.* **2021**, *42*, 290–293.
[27] J. H. Cavka, S. Jakobsen, U. Olsbye, N. Guillou, C. Lamberti, S. Bordiga, K. P. Lillerud, *J. Am. Chem. Soc.* **2008**, *130*, 13850–13851.
[28] L. Valenzano, B. Civalleri, S. Chavan, S. Bordiga, M. H. Nilsen, S. Jakobsen, K. P. Lillerud, C. Lamberti, *Chem. Mater.* **2011**, *23*, 1700–1718.

[29] M. Kaposi, M. Cokoja, C. H. Hutterer, S. A. Hauser, T. Kaposi, F. Klappenberger, A. Pöthig, J. V. Barth, W. A. Herrmann, F. E. Kühn, *Dalton Trans.* **2015**, *44*, 15976–15983.
[30] L. Feng, S. Yuan, J.-S. Qin, Y. Wang, A. Kirchon, D. Qiu, L. Cheng, S. T. Madrahimov, H.-C. Zhou, *Matter* **2019**, *1*, 156–167.
[31] Z. Hu, D. Zhao, *Dalton Trans.* **2015**, *44*, 19018–19040.
[32] M. J. Katz, Z. J. Brown, Y. J. Colón, P. W. Siu, K. A. Scheidt, R. Q. Snurr, J. T. Hupp, O. K. Farha, *Chem. Commun.* **2013**, *49*, 9449.
[33] Y. Bai, Y. Dou, L.-H. Xie, W. Rutledge, J.-R. Li, H.-C. Zhou, *Chem. Soc. Rev.* **2016**, *45*, 2327–2367.
[34] A. J. Blake, W.-S. Li, V. Lippolis, M. Schröder, F. A. Devillanova, R. O. Gould, S. Parsons, C. Radek, *Chem. Soc. Rev.* **1998**, *27*, 195.
[35] G. Kresse, J. Hafner, *Phys. Rev. B* **1993**, *47*, 558–561.
[36] J. Hafner, *J. Comput. Chem.* **2008**, *29*, 2044–2078.
[37] P. E. Blöchl, *Phys. Rev. B* **1994**, *50*, 17953–17979.
[38] G. Kresse, D. Joubert, *Phys. Rev. B* **1999**, *59*, 1758–1775.
[39] J. P. Perdew, K. Burke, M. Ernzerhof, *Phys. Rev. Lett.* **1996**, *77*, 3865–3868.
[40] S. Grimme, J. Antony, S. Ehrlich, H. Krieg, *J. Chem. Phys.* **2010**, *132*, 154104.
[41] J. Moellmann, S. Grimme, *Phys. Chem. Chem. Phys.* **2010**, *12*, 8500.
[42] S. Grimme, *WIREs Comput. Mol. Sci.* **2011**, *1*, 211–228.
[43] S. Chibani, M. Badawi, T. Loiseau, C. Volkringer, L. Cantrel, J.-F. Paul, *Phys. Chem. Chem. Phys.* **2018**, *20*, 16770–16776.
[44] S. Sircar, J. R. Hufton, *Adsorption* **2000**, *6*, 137–147.
[45] M. Streza, O. Grad, D. Lazar, M. Depriester, S. Longuemart, A. H. Sahraoui, G. Blanita, D. Lupu, *Int. J. Heat Mass Transf.* **2019**, *143*, 118539.
[46] M. W. Logan, S. Langevin, Z. Xia, *Sci. Rep.* **2020**, *10*, 1492.
[47] G. Blăniţă, M. Streza, M. D. Lazăr, D. Lupu, *Int. J. Hydrog. Energy* **2017**, *42*, 3064–3077.
[48] H. A. Benesi, J. H. Hildebrand, *J. Am. Chem. Soc.* **1949**, *71*, 2703–2707.
[49] R. S. Mulliken, *J. Phys. Chem.* **1952**, *56*, 801–822.
[50] G. DeBoer, J. W. Burnett, M. A. Young, *Chem. Phys. Lett.* **1996**, *259*, 368–374.
[51] F. Grozema C., R. Zijlstra W. J., M. Swart, P. Th. Van Durinen, *Int. J. Quantum Chem.* **1999**, *75*, 709–723.
[52] A. J. A. Baskar, A. S. Rajpurohit, M. Panneerselvam, M. Jaccobb, D. RoopSingh, V. Kannappan, *Chem. Data Collect.* **2017**, *7–8*, 80–92.
[53] A. Gładysiak, T. N. Nguyen, M. Spodaryk, J. Lee, J. B. Neaton, A. Züttel, K. C. Stylianou, *Chem. Eur. J.* **2019**, *25*, 501–506.
[54] F. Salles, J. Zajac, *Nanomaterials* **2021**, *11*, 2245.
[55] S. Chibani, F. Chiter, L. Cantrel, J.-F. Paul, *J. Phys. Chem. C* **2017**, *121*, 25283–25291.
[56] D. Banerjee, X. Chen, S. S. Lobanov, A. M. Plonka, X. Chan, J. A. Daly, T. Kim, P. K. Thallapally, J. B. Parise, *ACS Appl. Mater. Interfaces* **2018**, *10*, 10622–10626.
[57] L. Shen, R. Liang, M. Luo, F. Jing, L. Wu, *Phys. Chem. Chem. Phys.* **2015**, *17*, 117–121.
[58] L. A. Walker, S. Pullen, B. Donovan, R. J. Sension, *Chem. Phys. Lett.* **1995**, *242*, 177–183.
[59] S. S. Lobanov, J. A. Daly, A. F. Goncharov, X. Chan, S. K. Ghose, H. Zhong, L. Ehm, T. Kim, J. B. Parise, *J. Phys. Chem. A* **2018**, *122*, 6109–6117.
[60] R. I. Gray, K. M. Luckett, J. Tellinghuisen, *J. Phys. Chem. A* **2001**, *105*, 11183–11191.
[61] J. Tellinghuisen, *J. Phys. Chem. A* **2012**, *116*, 391–398.
[62] N. Li, L. Shi, X. Wang, F. Guo, C. Yan, *Int. J. Anal. Chem.* **2011**, *2011*, 1–7.

[63] J. M. Gardner, M. Abrahamsson, B. H. Farnum, G. J. Meyer, *J. Am. Chem. Soc.* **2009**, *131*, 16206–16214.
[64] K. Hendrickx, J. J. Joos, A. De Vos, D. Poelman, P. F. Smet, V. Van Speybroeck, P. Van Der Voort, K. Lejaeghere, *Inorg. Chem.* **2018**, *57*, 5463–5474.
[65] K. Hendrickx, D. E. P. Vanpoucke, K. Leus, K. Lejaeghere, A. Van Yperen-De Deyne, V. Van Speybroeck, P. Van Der Voort, K. Hemelsoet, *Inorg. Chem.* **2015**, *54*, 10701–10710.
[66] C. A. Téllez S, E. Hollauer, M. A. Mondragon, V. M. Castaño, *Spectrochim. Acta A Mol. Biomol. Spectrosc.* **2001**, *57*, 993–1007.
[67] Peter. Klaeboe, *J. Am. Chem. Soc.* **1967**, *89*, 3667–3676.
[68] W. Kiefer, H. J. Bernstein, *J. Raman Spectrosc.* **1973**, *1*, 417–431.
[69] A. Anderson, T. S. Sun, *Chem. Phys. Lett.* **1970**, *6*, 611–616.
[70] P. Deplano, F. Devillanova, J. Ferraro, F. Isaia, V. Lippolis, M. Mercuri, *Appl. Spectrosc.* **1992**, *46*, 1625–1629.
[71] R. P. Cooney, P. J. Hendra, M. Fleischmann, *J. Raman Spectrosc.* **1977**, *6*, 264–266.
[72] P. Deplano, J. R. Ferraro, M. L. Mercuri, E. F. Trogu, *Coord. Chem. Rev.* **1999**, *188*, 71–95.
[73] P. H. Svensson, L. Kloo, *Chem. Rev.* **2003**, *103*, 1649–1684.
[74] S. L. Hsu, A. J. Signorelli, G. P. Pez, R. H. Baughman, *J. Chem. Phys.* **1978**, *69*, 106.
[75] C. Wang, Y. Wang, R. Ge, X. Song, X. Xing, Q. Jiang, H. Lu, C. Hao, X. Guo, Y. Gao, D. Jiang, *Chem. Eur. J.* **2018**, *24*, 585–589.
[76] W. Zhang, Y. Mu, X. He, P. Chen, S. Zhao, C. Huang, Y. Wang, J. Chen, *Chem. Eng. J.* **2020**, *379*, 122365.
[77] W. F. Howard, L. Andrews, *J. Am. Chem. Soc.* **1975**, *97*, 2956–2959.
[78] A. G. Al Lafi, B. Assfour, T. Assaad, *J. Inorg. Organomet. Polym.* **2020**, *30*, 1218–1230.
[79] X. Zhang, I. da Silva, R. Fazzi, A. M. Sheveleva, X. Han, B. F. Spencer, S. A. Sapchenko, F. Tuna, E. J. L. McInnes, M. Li, S. Yang, M. Schröder, *Inorg. Chem.* **2019**, *58*, 14145–14150.